THE THERMAL EVOLUTION OF THE OUACHITA OROGEN, ARKANSAS AND OKLAHOMA FROM QUARTZ-CALCITE THERMOMETRY AND FLUID INCLUSION THERMOBAROMETRY

A Thesis

by

JENNIFER ANN PIPER

Submitted to the Office of Graduate Studies of
Texas A&M University
in partial fulfillment of the requirements for the degree of

MASTER OF SCIENCE

December 2011

Major Subject: Geology

The Thermal Evolution of the Ouachita Orogen, Arkansas and Oklahoma from Quartz-Calcite Thermometry and Fluid Inclusion Thermobarometry

THE THERMAL EVOLUTION OF THE OUACHITA OROGEN, ARKANSAS AND OKLAHOMA FROM QUARTZ-CALCITE THERMOMETRY AND FLUID INCLUSION THERMOBAROMETRY

A Thesis

by

JENNIFER ANN PIPER

Submitted to the Office of Graduate Studies of
Texas A&M University
in partial fulfillment of the requirements for the degree of

MASTER OF SCIENCE

Approved by:

Chair of Committee,	David Wiltschko
Committee Members,	Ethan Grossman
	Brent Miller
	Niall Slowey
Head of Department,	Andreas Kronenberg

December 2011

Major Subject: Geology

ABSTRACT

The Thermal Evolution of the Ouachita Orogen, Arkansas and Oklahoma from Quartz-Calcite Thermometry and Fluid Inclusion Thermobarometry. (December 2011)

Jennifer Ann Piper, B.S., San Diego State University

Chair of Advisory Committee: Dr. David Wiltschko

To understand the fluid temperature and pressure during the Ouachita orogeny, we used isotopic analysis of syntectonic veins and adjacent host material, quartz-calcite oxygen isotope thermometry and fluid inclusion analysis. The veins were at or near isotopic equilibrium with their host rocks; neither the host nor veins has been isotopically reset. The average isotopic variation in $\delta^{18}O$ between vein and host is 2.4 ± 1.7‰ and 0.7 ± 1.7‰ for quartz and calcite, respectively. The temperature of vein formation from quartz-calcite oxygen isotope thermometry is about 210°-430°C. Although this is a large range, the temperature does not vary systematically in the exposed Ordovician through Mississippian rocks. The lack of isotopic difference between host and vein suggests that the host oxygen determined that of the veins. This in turn suggests that the fluid in the rocks did not change regionally. The vitrinite reflectance/temperature of the host rocks increases with restored stratigraphic depth more than that calculated with the quartz-calcite thermometer in veins. Fluid inclusion analysis in vein quartz constrains homogenization temperatures to be from 106º-285ºC. Isochores from fluid inclusion analyses were constrained using quartz-calcite

thermometry and vitrinite reflectance temperatures to calculate vein formation pressures of 0.3–4.7 kbars. These pressures correspond to vein formation depths up to 19 km, assuming an unduplicated stratigraphic section. Using burial curves and a reasonable range of geothermal gradients, vein formation ages are between 300 to 315 Ma, i.e., Early to Middle Pennsylvanian.

ACKNOWLEDGEMENTS

We thank Dr. Ethan Grossman and Art Kasson from the Texas A&M University Stable Isotope Geoscience Facility for providing the time and technical expertise regarding stable isotope analyses of our calcite samples. We also thank Dr. Ian Richards and everyone at the Stable Isotope Laboratory at Southern Methodist University for their help and collaboration with stable isotope analyses in quartz. Dr. Mike Tice provided guidance and assistance when using the XRF, and Adam Cosentino provided assistance in using ArcGIS. We also would like to thank Dr. Will Lamb for providing the time and equipment for completing fluid inclusion analyses. Thanks also to Harold Johnson and Shay Chapman for field assistance in the Ouachitas. We would also like to acknowledge several sources of funding that have made this project possible: Devon Corporation, ExxonMobil Corporation, ConocoPhillips Spirit Scholarship program, and the American Association of Petroleum Geologists.

TABLE OF CONTENTS

Page

1. INTRODUCTION

Understanding the thermal history of the Carboniferous Ouachita orogeny in Arkansas and Oklahoma is a challenge due to an apparent Cretaceous heating event (Arne, 1992; Winkler et al., 1999). Specifically, apatite fission track dates from the core of the orogen are middle to late Cretaceous, rendering low-temperature thermochronometers useless in determining the timing and thermal conditions during the Ouachita orogeny (compare Burtner et al., 1994; Fuller et al., 2006).

Although directly dating the thermal history of the Ouachita orogeny might be out of reach at present, determining the temperature and pressure during deformation lends itself to several approaches. Houseknecht and Matthews (1985) and Guthrie et al. (1986) determined the thermal maturity of the Ouachita strata to be ~ 279º - 397ºC using vitrinite reflectance and illite crystallinity, respectively. Richards et al. (2002) and Cervantes and Wiltschko (2010) conducted stable isotope analyses on vein and host material and report an average difference of 2.4 ± 1.6‰ and ~2‰, respectively. Using quartz-calcite isotope fractionation of cogenetic minerals Richards et al. (2002) determined that the temperature of vein formation was 83º - 385ºC, using the calibrations of Clayton et al. (1989) and Sharp and Kirschner (1994). Homogenization temperatures from fluid inclusions are reported to be between 120º - 267ºC (Engel, 1952; Konig and Stone, 1977; Keller et al., 1985; Shelton et al., 1986; Cervantes and

---

This thesis follows the style of the Journal of Structural Geology.

Wiltschko, 2010). However, as all fluid inclusion fillings found to date are aqueous fluid and vapor, an independent pressure constraint is needed to determine the temperature (e.g., Roedder, 1984). Shelton et al. (1986) used conodont color alteration indices to constrain a pressure of vein formation of 1.9 kbar.

The purpose of this study is to determine the formation temperature and pressure of syntectonic veins in the oldest and most intensely deformed rocks exposed in the Benton and Broken Bow uplifts of Oklahoma and Arkansas. We do this by integrating the published thermochronology, thermal maturation and isotopic data referred to above with new quartz-calcite thermometry and fluid inclusion results.

We proceed in the following way. Published thermal maturation data provide the maximum temperatures for the host rocks. Vein precipitation temperatures are determined from the quartz-calcite thermometer. If the host and vein temperatures are the same, then host and vein thermal histories may be the same. Next, the vein temperatures are used to constrain the pressure of vein formation from fluid inclusion isochores. The resulting pressures are then compared to the pressure calculated from the reconstructed overburden. If we assume overburden is normal stratigraphic thickness without structural thickening, we can infer a depth at the time of vein formation. Alternatively, we can test whether the no structural stacking assumption is correct. Finally, we convert the vein temperature and pressure to burial depth and find the times during the burial history of the Ouachitas when the veins could have formed.

2. GEOLOGIC BACKGROUND

2.1. Regional Setting

The Ouachita orogen is part of a series of exposures of Paleozoic rocks that extends from the southwestern edge of the Appalachian Mountains to Arkansas (Ouachita Mountains), through Texas (Marathon uplift) and into Mexico (Fig. 1). The subsurface connection between these exposures has been established by reflection seismic and drilling and is located schematically on Figure 1 as the "Frontal Thrust Belt". The orientation of these exposures defines the trend of a late Paleozoic collisional belt (e.g., Stone et al., 1982; Arbenz, 1989; Nielsen et al., 1989; Viele and Thomas, 1989; Poole et al., 2005). We refer to this orogen collectively as the Ouachita-Marathon collision belt (OMCB). The Wichita Mountains, Arbuckle Mountains and Llano uplift are in the foreland, cratonward of the OMCB (Fig. 1). We define the Ouachita core as the oldest and hottest exposed rocks in the Benton and Broken Bow uplifts of southwestern Arkansas and southeastern Oklahoma (Fig. 1, 2). Today, post-orogenic Permian, Mesozoic and Cenozoic rocks of the Mississippi Embayment and the Coastal Plain onlap separate exposures of the OMCB.

2.2. Tectonic History

The tectonic history of the Ouachita orogen is not well understood because much of the rock record is buried beneath the post-orogenic Mississippi Embayment and Coastal Plain onlap. Most workers agree that the Appalachian and OMCB lie along the

early Paleozoic southern margin of the North American continental crust, which was shaped by the breakup of Rodinia (e.g., Keller and Cebull, 1973; Cebull et al., 1976; Stewart, 1976; Thomas, 1976; Kruger and Keller, 1986; Arbenz, 1989; Nielsen et al., 1989; Viele and Thomas, 1989; Thomas, 1991; Poole et al., 2005). From the late Cambrian to early Mississippian the Ouachita region of Laurentia was a south-facing, passive continental margin (e.g., Nelson et al., 1982; Lillie et al., 1983; Arbenz, 1989). Sedimentation rates abruptly increased in the adjacent foreland basin during the middle Mississippian, which is taken as the onset of the Ouachita orogeny (e.g., Dickinson, 1974; Arbenz, 1989; Morris, 1989; Viele and Thomas, 1989). The orogeny was caused by the collision of the North American plate with an unknown landmass that has been variably identified as Gondwana (e.g. Arbenz, 1989; Whitaker and Engelder, 2006), a volcanic arc (e.g. Graham et al., 1975) or an unknown continent (e.g., Briggs and Roeder, 1978; Nelson et al., 1982; Lillie et al., 1983). During the orogeny, turbiditic and hemipelagic muds and silts accumulated in basins adjacent to the OMCB (e.g., Viele and Thomas, 1989). Syntectonic sediments deposited in the foreland basin to the north of the Ouachita orogen are now part of the Arkoma basin. Seismic reflection profiles show that 7-12 km of sediments exist south of the exposed Ouachita orogen (Figure 3; Nelson et al., 1982; Lillie et al., 1983). High sedimentation rates continued until the early Permian, which is when deformation is believed to have ended (Nelson et al., 1982; Lillie et al., 1983; Viele and Thomas, 1989).

The Ouachita core is defined as a north-northeast trending anticlinorium defined by the Benton and Broken Bow uplifts (Figs 2 and 3). The predominant structures in the

Ouachita core are north to northwest verging thrust sheets and upright to recumbent folds (e.g., Poole et. al., 2005; Whitaker and Engelder, 2006). Locally, thrust faults are overturned on the north flank of the uplifts (e.g., Haley and Stone, 1996). Paleozoic rocks in both the Broken Bow and eastern portion of the Benton uplifts have undergone greenschist grade metamorphism and are characterized by extensive veining (e.g. Honess, 1923; Goldstein and Reno, 1952; Nielsen et al., 1989; Viele and Thomas, 1989).

The rocks in the Benton uplift experienced post-orogenic extension, as indicated by late normal faults that offset Paleozoic rocks in the subsurface (e.g. Hildenbrand et al., 1982; Lillie et. al., 1983; Kruger and Keller, 1986). Some workers attribute normal faulting to rifting during the opening of the Gulf of Mexico in the late Permian to Triassic (e.g. Lillie et. al., 1983). Finally, the late Paleozoic rocks were buried by Cretaceous to Quaternary sediments along the Gulf Coast and in the Mississippi Embayment (e.g. Curtis, 1991).

2.3. Stratigraphy

As shown in Figure 4 the sediments may be divided into pre- and syn-orogenic deposits (e.g. McBride, 1975; Stone et al., 1982; Lowe, 1989; Poole et. al., 2005). Pre-orogenic sediments include Ordovician through lower Mississippian strata (Collier Shale through Arkansas Novaculite). These sediments consist of carbonate shelf to abyssal plain deposits that accumulated at low sedimentation rates (e.g. McBride, 1975). Syn-orogenic sediments include Mississippian through middle Pennsylvanian strata (Stanley Shale through the Atoka Formation) and are dominated by deep-water flysch deposits

(e.g. Johnson et al., 1988; Morris, 1989). During this phase, large amounts of clastic sediment were deposited as turbidite fan complexes (e.g. Arbenz, 1989). The transition from pre- to syn-orogenic sedimentation is marked by an increase in sedimentation rates (e.g. Arbenz, 1989; Viele and Thomas, 1989) at the basal contact of the Stanley shale. This contact is not easily identified in outcrop due to both the amount of shortening and the lack of exposure.

2.4. Veins

There are two broad types of veins in the Ouachitas; generally small syntectonic veins and large commercial (post-tectonic) veins filled with prismatic clear quartz and milky calcite crystals. Veins are found in Ordovician to Mississippian shales, limestones and sandstones of the Benton and Broken Bow uplifts. The most heavily veined portions of the Ouachita core form a ~50 - 65 km wide by 270 km long region that has been termed the vein-quartz belt (e.g. Miser, 1943, 1959; Richards et al., 2002; Fig. 2).

Syntectonic veins contain milky quartz with varying amounts of calcite, mica and feldspar. They are small, < 1 cm to ~ 5 cm in width, with fibrous to blocky textures. Syntectonic veins are slightly to highly deformed and tend to follow the orientation of nearby structural features (e.g. Honess, 1923; Stone and Haley, 1994). Vein deformation includes, but is not limited to, faulting, folding and internal crushing. Other evidence of syntectonic vein formation is calcite twinning seen in thin sections. There does not appear to be a regional or stratigraphic pattern to vein deformation intensity.

Commercial veins are vuggy, up to 30 m wide, with large, clear quartz crystals that are mined and sold worldwide (e.g. Engel, 1952; Stone and Haley, 1994). They are undeformed and crosscut structural features from the Ouachita orogeny, meaning that they are post-tectonic (e.g. Miser, 1943; 1959). The precise age is unknown. Other studies have acknowledged the different types of veins but do not specifically state which were analyzed or how they determined which are which (e.g., Shelton et al., 1986; Richards et al., 2002).

The timing of syntectonic veins is not certain but is believed to be late in the Ouachita orogeny because they are mostly mildly deformed while their host rocks are more highly deformed (e.g. Honess, 1923; Stone and Haley, 1994). There are two sets of dates for Ouachita veins. Bass and Ferrara (1969) dated adularia in veins from the Ouachitas using Rb-Sr and K-Ar and obtained ages of 287 - 279 Ma and 214 - 190 Ma, respectively. They combined these ages with isotopic, stratigraphic and structural data and reported an overall age of formation of late Pennsylvanian to early Permian (Bass and Ferrara, 1969). Similarly, Shelton et al. (1986) dated adularia from veins in the Womble shale using K-Ar and obtained an age of 262 Ma.

3. PREVIOUS WORK ON THE THERMAL REGIME

3.1. Vitrinite Reflectance

The first constraints on the thermal state of host rocks making up the Ouachita orogen were determined using vitrinite reflectance (Houseknecht and Matthews, 1985; Guthrie et al., 1986). Vitrinite reflectance yields the thermal maturity of organic matter in sedimentary rocks based on the light reflectance of vitrinite found in coal or other organic matter. The vitrinite group of kerogen is used because it is sensitive to small temperature changes and its optical properties change uniformly during catagenesis (e.g. Dow, 1977). Ro refers to the 'percent reflectance in oil' because the measurements are made with oil immersion objectives on a reflecting microscope (e.g. Dow, 1977; Heroux et al., 1979).

Vitrinite reflectance data from the Ouachita orogen reveal a large range in thermal maturity both geographically and stratigraphically (Houseknecht and Matthews, 1985; Guthrie et al., 1986). Rocks from the Benton uplift have a higher thermal maturity (Ro = 2.5 - > 4.0%) than those in the Broken Bow uplift (Ro = < 2.0 - 3.0%; Fig. 5). Using the vitrinite maturation model of Price (1983), the Ro values are equivalent to maximum paleotemperatures of 308°- 370°C and 279°- 332°C in the Benton and Broken Bow uplifts, respectively. The Ro values of pre-Carboniferous strata in the Ouachita core are 3.0 – 4.9% (Houseknecht and Matthews, 1985), with maximum paleotemperatures of 332º - 397ºC (Price, 1983). Figure 5 shows that Ro values reach a maximum in the eastern Benton uplift and decrease to the north and south away from the

core in conjunction with decreasing stratigraphic ages of exposed rocks. This pattern in thermal maturity is believed to be a result of increasing overburden and subsequent erosion of the Ouachitas from west to east (Byrnes and Lawer, 1999). Byrnes and Lawer (1999) use 115 well locations and simple burial models to show that Ro increases with present depth, presumably as a result of stratigraphic burial.

3.2. Apatite Fission Track Dating

Apatite fission track (AFT) ages from the Ouachita orogen are up to 100 Ma younger than the depositional age of the unit from which the apatite grains were sampled (e.g. Arne, 1992; Corrigan et al., 1998; Winkler et al., 1999). Winkler et al., (1999) constructed a thermal history model for the Ouachita, Marathon, Llano, Arbuckle and Wichita exposures using AFT data. Their thermal history model, shown in Figure 6, is made to fit data from both the foreland basin (Llano, Arbuckle and Wichita) and the OMCB 40 to 400 km away. The model starts with the assumption that rocks in the foreland basin were near the surface in the early Permian (Winkler et al., 1999). AFT data from the foreland suggest that these rocks were heated above the apatite partial annealing zone after the Ouachita orogeny, ~300 - 270 Ma (Winkler et al., 1999). AFT data from the OMCB suggest that there was significant cooling in the Late Jurassic to the early Cretaceous (to ~20°- 30°C), coincident with the opening of the Gulf of Mexico (Arne, 1992; Winkler et al., 1999). This cooling was followed by middle to late Cretaceous heating (up to ~80°C), then Tertiary cooling to the present (Winkler et al., 1999).

Middle to late Cretaceous heating is based on fission track length and age data from the Marathon and Benton uplifts in the OMCB (Winkler et al., 1999). AFT data provide no constraints on the thermal history of these areas prior to the late Jurassic (Winkler et al., 1999). This means that the extent and timing of Pre-Jurassic heating is not known in the OMCB.

These heating events are not evident throughout the Appalachian Mountains. For example, AFT data from the central Appalachians (Pennsylvania, Maryland, West Virginia and Virginia) suggest a thermal history that starts with heating during the late Permian (~250 Ma) and slow cooling to the present (dashed lines in Figure 6) (e.g. Roden and Miller, 1989; Roden, 1991; Blackmer et al., 1994). Figure 6 shows that the thermal histories of the Ouachitas and the central Appalachians reasonably coincide from the Permian until the early Cretaceous (e.g. Roden and Miller, 1989; Roden, 1991; Blackmer et al., 1994; Winkler et al., 1999). The two regions differ in the early Cretaceous when the Ouachitas experienced a second heating while the central Appalachians continued to cool (Figure 6). Comparison to the central Appalachians is hampered by geographic distance and varying geology, making any comparison of thermal histories tentative at best. However, Naeser et al. (2006) report regional cooling in eastern Tennessee and the western Carolinas beginning no later than the late Triassic to early Jurassic and continuing through the Cretaceous, similar to the central Appalachians.

3.3. Stable Isotopes

Richards et al. (2002) show that isotopic values from the Ouachita veins and adjacent hosts they studied vary by lithology. Specifically, $\delta^{18}O$ values of veins and their hosts are similar in quartz-rich units (Arkansas Novaculite, Blaylock Sandstone, Polk Creek Shale and Bigfork Chert; see Fig. 4). Similarly, $\delta^{13}C$ values of veins and their hosts are similar in calcite-rich units (Stanley, Womble and Mazarn Shales). The vein-host similarity suggests that the source of vein C and O is the adjacent host for calcite- and quartz-rich lithologies, respectively. On the other hand, there is significant variability between vein and host $\delta^{18}O$ values in calcite-rich lithologies. For these reasons, Richards et al. (2002) postulated a complex fluid flow model with a distal source that diffused through the host rock, causing the isotopic values of the veins to reflect those of the host in some cases and a shift in others.

Richards et al. (2002) also use quartz-calcite isotope fractionation to calculate vein formation temperatures of 265º - 385ºC using the equation from Sharp and Kirschner (1994) and 83º - 163ºC using Clayton et al (1989). The differences in the computed temperatures are a result of the different fractionation factors used in the two studies for quartz and calcite. Which equation is preferable is an open question. Each one is discussed in detail in section 5.4 below.

3.4. Fluid Inclusions

Early studies of fluid inclusions in the Ouachita orogen provide homogenization temperatures but were not able to obtain formation pressure or temperature because

independent constraints were unavailable. Engel (1952) reports homogenization temperatures of 120° - 175°C from vein quartz in commercial quartz crystal mines. Konig and Stone (1977) report homogenization temperatures of 190° - 267°C from fluid inclusions in milky quartz veins in the northeastern frontal Ouachitas. Keller et al. (1985) report homogenization temperatures of ~200°C from fluid inclusions in quartz veins within the Arkansas novaculite of the Benton Uplift. Homogenization temperatures from an outcrop in Hot Springs, AK range from 103º - 247ºC (Cervantes and Wiltschko, 2010). Unfortunately, homogenization temperatures alone do not tell us much about the thermal history of vein formation, as they can only provide an isochore with a range of possible formation temperatures and pressures.

In order to constrain both temperature and pressure, an independent estimate of one or the other is needed. A study by Shelton et al. (1986) combines homogenization temperatures from fluid inclusions with an estimate of the maximum burial temperature from conodont color alteration indices (CAI). The CAI is an experimentally determined color scale for the maximum temperature of exposure. The color changes are calibrated at 50°C increments from 300°- 600°C (Rejebian et al., 1987; Helsen et al., 1995). Shelton et al. (1986) report homogenization temperatures from veins within the Womble Shale near Lake Ouachita of 131° - 157°C with salinities between 0.9 and 3.7 wt% NaCl equivalent. The maximum temperature of the host was constrained to ~300°C by the conodont CAI. With this maximum temperature constraint, Shelton et al. (1986) computed a maximum pressure of vein formation of 1.9 kbar. This corresponds to a maximum depth of ~7.6 km, assuming lithostatic pressure (Shelton et al., 1986).

4. SAMPLES AND METHODS

4.1. Sample Collection

To further constrain the thermal evolution of the Ouachita orogen, we sampled syntectonic veins and their adjacent host rocks from Ordovician to Pennsylvanian rocks throughout the Ouachita orogen in Arkansas. Sample locations are shown in Figure 2. We concentrated on thin (< 1 cm to ~ 5 cm) veins that were deformed (folded, faulted) or were structurally related to the larger structure that contained them. Because nearly all veins display wall-normal dilation, veins oriented either normal or parallel to fold axes were preferred over those at other orientations. In some cases, it was difficult to determine in the field if a vein was syntectonic, but care was taken not to sample any of the vuggy, undeformed commercial veins. Due to the quality of exposure, most samples came from road-cuts and lakeside outcrops. Additional outcrops were found using sample localities of Richards et al. (2002). Veins containing both quartz and calcite are rare to the north and south of the Ouachita core. In total, fifty-seven samples were collected along the east-west trend of the Ouachita core, twenty of which have both quartz and calcite.

4.2. Vein Texture: Optical and X-Ray Fluorescence Methods

Standard thin sections and X-Ray Fluorescence (XRF) were used to determine if quartz and calcite are co-genetic and therefore suitable for the quartz-calcite thermometer. In addition to petrographic thin sections, seven typical samples were

slabbed and element maps were produced on the Horiba XGT-7000 X-ray fluorescence micro-analyzer (XRF) at Texas A&M University. The XRF is capable of semi-quantitative and quantitative imaging of elements from Na to U in samples with dimensions up to 5 x 5 x 3 cm. It has a spot size of 10 or 100 μm and a detection limit of 50 - 100 ppm for Na to U. All samples were cut to the above dimensions or smaller and were analyzed using a spot size of 100 μm. The XRF records a full elemental spectrum in each pixel of the selected sample area. The elemental maps are 2.5 cm^2. *Image J* software was used to combine black and white images of single elements from the XRF into a colored image displaying all of the elements of interest.

4.3. Stable Isotopes

Stable isotope analyses of carbon and oxygen in quartz and calcite were measured from veins and their adjacent host rocks throughout the Ouachitas. For calcite analysis, 10 mg of calcite was drilled from both the vein and the host material using a micro-drill. Sixty samples were then weighed and analyzed on the MAT 253 isotope ratio mass spectrometer (IRMS) using a Kiel automated carbonate reaction system in the Texas A&M University Stable Isotope Geoscience Facility. For quartz samples, at least 30 mg of quartz was chipped out from grains adjacent to the sampled calcite grains. For thin veins with small crystals, several quartz grains were sampled to get the required sample size. Forty-six samples were crushed to a fine sand grain size (125 - 250 μm) using a marble mortar and pestle. Clay particles were removed using forceps under the microscope. The quartz samples were treated with 0.6 N HCl two to three times for

decarbonization. Once dry, the samples were run through the O_2 extraction line following the method of Clayton and Mayeda (1963), and analyzed on the Finnigan MAT 252 IRMS in the Stable Isotope Laboratory at Southern Methodist University.

Stable isotope compositions are reported as δ-values defined by,

$$\delta = (R_{sample}/R_{standard} - 1) \times 1000 \quad (1)$$

where R is either $^{18}O/^{16}O$ or $^{13}C/^{12}C$ relative to Vienna Standard Mean Ocean Water (VSMOW) for oxygen and Peedee belemnite (VPBD) for carbon. Replicate analyses of the carbonate standard NBS-19 gave average values of $\delta^{13}C = 1.95 \pm 0.03‰$ and $\delta^{18}O = 28.6 \pm 0.09‰$. Replicate analyses of the quartz standard NBS-28 gave an average $\delta^{18}O$ of $9.6 \pm 0.15‰$. These uncertainties are based on the standard deviation (1σ) of the replicate standards.

4.4. Fluid Inclusions

Primary fluid inclusions (Roedder, 1984) from ten samples were measured in order to obtain the composition and density of the fluid present during vein formation. The phase transition temperatures of 242 fluid inclusions were measured on polished thick sections using a heating and cooling stage (Werre et al., 1979). These temperatures were then compared to experimentally determined phase relations for various fluids and mixtures to determine the compositions and densities of the fluid inclusions. Melting temperature (T_m) is most closely related to salinity and the homogenization temperature (T_h) is related to density. With this information an isochore (a range of pressure and temperature conditions under which the fluid inclusions could have formed) was

constructed for each sample using the methods described by Mao and Duan (2008). Salinities, compositions and isochores were determined using online fluid inclusion analysis software from The Zhenhao Duan Research Group (http://calc.geochem-model.org/Pages/H2ONaCl.aspx). Quartz-calcite isotope thermometry and vitrinite reflectance values were used as independent temperature constraints in order to identify the range of pressure conditions possible for vein formation in the Ouachitas.

4.5. Vitrinite Reflectance Temperature Calculation

A vitrinite reflectance (Ro) value for each of our samples was obtained by extrapolating values from the Ro contour map of Houseknecht and Matthews (1985). For each data point the Ro value was estimated with an assumed error of ± 0.5%. We choose this error because the Ro contour interval on the map is 1.0%. The Ro values for each sample were then converted to maximum temperatures using the relationship of Price (1983). These temperatures are used to constrain the maximum host rock temperature and are used to calculate maximum depths for different geothermal gradients. The maximum depths for the host rocks also give the maximum depth possible for vein emplacement. These temperatures can also be used with fluid inclusion isochores to predict the maximum pressure of vein formation, assuming that the vein and host rock are in equilibrium.

Vitrinite reflectance values may be converted to maximum temperatures by using a vitrinite maturation model. The vitrinite maturation model of Price (1983) is based on a linear regression analysis of vitrinite reflectance versus burial temperatures from several

sedimentary basins throughout the Texas – Louisiana Gulf Coast. Price (1983) shows that the correlation coefficient between Ro and burial temperature in Gulf Coast basins is 0.97. The least-squares fit for data compiled by Price (1983) is

$$T = 302.97 \log_{10} R_o + 187.33 \quad (2)$$

where T is temperature in ºC. The conversion of R_o values to temperature only provides a maximum temperature. It does not provide information on the timing or duration of the heating and cannot distinguish between multiple and single heating events. Rocks that experienced high temperatures for a short duration can display the same reflectance values as rocks that were exposed to lower temperature for longer periods of time (Price, 1983). Data in Price (1983) suggests that rocks held at temperature less than 1 m.y. do not subsequently change Ro. Therefore, events shorter than 1 Ma cannot be resolved. For the rocks of the Ouachitas, this kinetic lag effect is judged as insignificant.

5. RESULTS

5.1. Vein Texture and Quartz-calcite Equilibrium

Quartz-calcite isotope thermometry requires that mineral pairs be co-genetic (Clayton et al., 1989; Sharp and Kirschner, 1994). Thin section and X-ray fluorescence analysis were used to determine if quartz and calcite are in textural equilibrium and hence, more likely also to be in isotopic equilibrium.

Thin section observations confirm the presence of varying amounts of quartz and calcite (Fig. 7) with blocky (Fig. 7A-F) to fibrous (Fig. 7G) textures. Thin section observations also show that quartz and calcite are intimately related and have both sharp (Fig, 7A) and feathered grain boundaries (Fig. 7B). It is possible that quartz and calcite are not cogenetic but most textural observations support equilibrium growth (interdigitated quartz and calcite grains). All of the vein samples observed in thin section have evidence of deformation, be it calcite twinning (Fig. 7C-D) or healed fractures in quartz grains (Fig. 7E-F). Although the timing of mechanical twinning is not known, the existence of twinned calcite grains supports the interpretation that the veins containing these grains are pre- or syn-tectonic.

Figure 8 displays seven typical vein XRF element maps and photos of their corresponding hand specimens. For our purposes the element calcium is representative of calcite and silicon represents quartz. The XRF images show quartz veins (Fig. 8C-D), calcite veins (Fig. 8E) and mixtures of both (Fig. 8A, B, F, G). The trend of changing composition from the vein-host wall to the vein center is also observed in the XRF

images. For example, sample E in Figure 8 is a calcite vein with quartz crystals along the vein-host boundary and sample G is mostly quartz with calcite crystals along the vein-host boundary. Overall, the veins we sampled display textures in both thin section and XRF that supports co-precipitation of quartz and calcite.

5.2. Stable Isotope Analysis

One hundred and forty isotope analyses were conducted from quartz and calcite veins and their adjacent host rocks from throughout the Ouachita orogen (Fig. 9; Table 1). Our data are represented by the black-filled symbols in Figure 9, and the data of Richards et al. (2002) are shown as gray-filled symbols for comparison. Overall, all of our carbonate isotopic data lie within one standard deviation of the mean isotope values of Richards et al. (2002). The $\delta^{18}O$ values of vein and host quartz are within two standard deviations of the mean reported by Richards et al. (2002; see Table 2).

The $\delta^{18}O$ values of samples for which both vein and host quartz were measured have a range of 14.9 - 19.3‰ and 13.7 - 16.5‰, respectively, and are shown as the black-filled symbols in Figure 9A. For some samples quartz was measured in the vein or host but not both. These samples have a range of $\delta^{18}O$ values of 13.7 - 25.0‰ for veins and 11.8 - 16.5‰ for host. Samples that fall on the 1:1 line in Figure 9A have equal vein and host $\delta^{18}O$ values. By contrast, the best-fit line through all of the data has a slope of 0.69 and a R^2 value of 0.72. Most vein $\delta^{18}O$ values are slightly heavier than the adjacent host, with an average difference of 2.4‰ (also shown in inset histogram). The difference can be as large as 7.6‰ and is greatest for samples with the isotopically lightest host.

The $\delta^{18}O$ values of vein and adjacent host calcite range from 14.0 - 21.4‰ and 15.1 - 21.8‰, respectively (black-filled symbols, Fig. 9B). The mean vein calcite is lighter than mean vein host with an average difference of 0.71‰ (Fig. 9B).

The $\delta^{13}C$ values of vein and host calcite in Figure 9C range from -4.2 - 0.9‰ and -5.2 - 1.0‰, respectively. One sample from this study (AR112) and three from Richards et al. (2002; Ms5-1V1, Ms5-1V2 and Ms5-2) have host calcite $\delta^{13}C$ values that are less than -10‰. These outliers are plotted in the inset graph of Figure 9C and are not included in the above data ranges. All of theses samples are from the same outcrop near Hot Springs, AR (see Fig. 2). The conclusion from Figure 9C is that all vein and adjacent host $\delta^{13}C$ are generally equal with an average difference of 0.38‰.

The $\delta^{18}O$ difference between vein calcite and adjacent host calcite is about the same as the $\delta^{13}C$ difference (Fig. 9D). The largest variation between host and vein calcite $\delta^{18}O$ and $\delta^{13}C$ is observed in shale dominated host rocks and is up to ~7‰ and ~4‰, respectively (Fig. 9D).

The $\delta^{18}O$ fractionation between quartz and calcite in this study ranges from -5.3 - 3.8‰ (Fig. 9E). For reference, we have plotted on Figure 9E a line with slope of 1 that represents equal quartz and calcite $\delta^{18}O$. Quartz-calcite values that fall below this line represent positive fractionation in $\delta^{18}O$ between these two minerals. Of the 33 mineral pairs we analyzed, 52% display positive fractionation. Our samples with positive quartz-calcite fractionations yield fractionations between 0.8 - 3.8‰, averaging 1.9‰ (Fig. 9F). When the data of Richards et al. (2002) are combined with our data, the positive $\delta^{18}O$

fractionation between quartz and calcite ranges from 0.8 - 4.4%, with an average of 2.4‰. With the larger data set, 99 mineral pairs were analyzed and 77% yielded a positive fractionation.

5.3. Quartz-calcite Thermometry

To determine the temperature of vein formation we use the quartz-calcite thermometer. The oxygen isotopic fractionation between quartz and calcite at equilibrium is temperature dependant. Because quartz prefers heavier oxygen isotopes than calcite during co-genetic crystallization (^{18}O versus ^{16}O), veins with a positive quartz-calcite isotopic fractionation are consistent with both minerals precipitating in equilibrium with the same fluid (e.g. O'Neil, 1986; Zheng, 1993; Sharp, 2007). This fractionation results from differences in bond strength of the oxygen isotopes, in particular the heavier isotope (^{18}O) will form a stronger bond and will have a higher bond energy (e.g. Sharp, 2007). Bond strengths are higher for the lighter elements, which is why quartz, mostly ^{14}Si, contains heavier isotopes than calcite, mostly ^{20}Ca (Zheng, 1993; Sharp, 2007). The oxygen fractionation is used to calculate the temperature of formation of the quartz-calcite mineral pair.

There are several equations in the literature used to calculate precipitation temperatures from quartz-calcite oxygen isotope fractionation. The two most commonly used relations are the experimentally derived equation from Clayton et al (1989) and the empirically derived equation from Sharp and Kirschner (1994). These two equations yield significantly different fractionation factors, which lead to significant differences in

temperature estimates and interpretations. The empirical relation of Sharp and Kirschner (1994) was calibrated using measured quartz and calcite $\delta^{18}O$ values from low-grade metamorphic rocks in the Swiss Alps with independently determined formation temperatures. Their equation is

$$1000 \ln \alpha_{QC} = 0.87 \times 10^6 T^{-2} \quad (3)$$

where α_{QC} is the fractionation factor for quartz-calcite equilibrium $[(^{18}O/^{16}O)_{quartz}/(^{18}O/^{16}O)_{calcite}]$ and T is temperature in °K. The term $1000 \ln \alpha_{QC}$ is approximated by $\delta^{18}O_{quartz} - \delta^{18}O_{calcite}$. The experimentally determined relation of Clayton et al. (1989) is

$$1000 \ln \alpha_{QC} = 0.38 \times 10^6 T^{-2} \quad (4)$$

This relationship was derived from direct-exchange experiments between calcite and quartz at specified temperatures. The discrepancy between these calibration methods is an ongoing debate. As discussed by Sharp (2007), some workers believe that the field calibrated technique is correct while others favor the laboratory experiments. At this point, it is unclear which method is best, therefore temperature ranges from both will be presented.

Formation temperatures were calculated from samples with positive quartz-calcite fractionation values. Negative fractionation indicates that the two minerals did not precipitate from the same fluid at the same temperature (O'Neil, 1986; Zheng, 1993; Sharp, 2007). Samples with negative fractionations occur throughout the Ouachitas and are not limited to one specific area or formation. Disequilibrium between quartz and calcite can occur when calcite is formed as a secondary mineral or is reset by isotope

exchange with water of different isotopic composition after formation (Kirschner et al., 1995). Some of the calcite samples with negative quartz-calcite fractionations appear weathered, which could affect the isotopic composition and negate quartz-calcite equilibrium. However it is often difficult, if not impossible, to identify which samples have equilibrium quartz and calcite from hand specimens alone. Separating samples by positive and negative quartz-calcite fractionations is one more way to improve the confidence in having done so.

The Clayton et al. (1989) equation yields precipitation temperatures of 47° - 415°C and the Sharp and Kirschner (1994) equation gives precipitation temperatures of 211° - 767°C (Fig. 13). The range of formation temperatures reported by Richards et al. (2002) is smaller because they only calculated the temperatures for samples with fractionations of 2 - 3‰. This is the range of the majority of their data and excludes all outliers. Their reported temperature estimates are 83° - 163°C using Clayton et al. (1989) and 265° - 385°C using Sharp and Kirschner (1994). These temperature ranges are meaningful if we assume that all of the veins in the Ouachitas were formed at the same time and under the same or similar conditions. When all of the data with positive quartz-calcite fractionations from Richards et al. (2002) are used the temperatures ranges are 25° - 219°C using Clayton et al. (1989) and 178° - 471°C using Sharp and Kirschner (1994; Fig. 13).

All of the calculated vein formation temperatures (this study and Richards et al., 2002) are plotted along trends parallel and perpendicular to the trend of the Ouachita core in Figure 10. The combined temperatures are 25° - 219°C (Clayton et al., 1989) and

178° - 471°C (Sharp and Kirschner, 1994) in all locations except for one (Fig. 10). The anomalous location has temperatures up to 415°C (Clayton et al., 1989) and 767°C (Sharp and Kirschner, 1994) and includes samples AR81, AR129 and AR130. All of these samples are from an outcrop approximately 15 km west of Lake Ouachita. The cause of this high temperature area is unknown. Richards et al. (2002) also have samples (Oc12) with extremely high formation temperatures from this area, but the samples are not shown because they have negative quartz-calcite fractionation factors. Excluding the outliers, the temperature ranges for our data alone are 47° - 191°C (Clayton et al., 1989) and 211° - 429°C (Sharp and Kirschner, 1994).

Not only do temperatures show no regional variation (excluding the one anomalous area west of Lake Ouachita), but there is also very little stratigraphic variation as well. Figure 11 shows the vein formation temperature variation in each formation with increasing depth. Vein formation temperatures from Sharp and Kirschner (1994) show similar temperatures in each formation with an average of 321º ± 47ºC, (shown by vertical dashed line in Fig. 11). In comparison, vitrinite reflectance temperatures from host rocks slightly increase with depth (Fig. 11). However, as shown on Figure 11, the errors in the quartz-calcite thermometry results are large enough to permit a normal increase in temperature with depth at about 24°C/km. Except for the topmost thermal maturation determination, the vitrinite reflectance results follow the same trend.

5.4. Fluid Inclusions

Two hundred and forty two primary fluid inclusions were measured in quartz grains from ten samples (Table 3). All fluid inclusions are two-phase water-rich inclusions with water vapor bubble sizes ranging between 5 - 40% by volume. Fluid inclusions vary in size (14.7 - 687.2 μm^2, assuming an elliptical shape), shape (rounded, elliptical or irregular) and frequency (isolated to densely spaced inclusions). For example, sample AR115 contains rounded inclusions while sample AR128 has irregular shaped inclusions (Fig 7H). Fluid inclusions in calcite are too small for fluid inclusion analysis.

Melting temperatures range from -10.9º to -0.1ºC with an average of -3.5º ± 2.4ºC (Fig. 12A). Homogenization temperatures range from 106º - 285ºC with an average of 176º ± 40ºC (Fig. 12B). Fluid inclusion salinities varied from 0.2 - 14.9 weight % NaCl equivalent with an average of 5.5 ± 3.4 weight % NaCl equivalent (Fig. 12C). The range in homogenization temperatures for each sample is shown in Figure 13, with the samples in approximate west (top left) to east (bottom right) order. The average homogenization temperature slightly increases to the east.

Isochores are plotted for each sample in Figure 14 using the highest, lowest and average homogenization temperatures for each sample. The range in homogenization temperatures observed in some samples causes the computed isochors to have varying slopes. We also see an increase in the dispersion of homogenization temperatures from west (AR136) to east (AR117). The range in homogenization temperatures for our

samples is only slightly larger than the previously reported range of 103º - 267ºC (Engel, 1952; Konig and Stone, 1977; Keller et al., 1985; Shelton et al., 1986).

5.5. T, P and Depth

By combining quartz-calcite isotope thermometry, vitrinite reflectance temperatures and fluid inclusion data we can constrain the temperature and pressure conditions during vein formation. Quartz-calcite $\delta^{18}O$ fractionations in veins allows for the temperature of vein formation to be calculated for each sample using the equations of Clayton et al. (1989) and Sharp and Kirschner (1994). Unfortunately, isotopic temperatures could not be calculated for all the samples with fluid inclusions due to the absence of calcite. Only two of the fluid inclusion samples (AR96 and AR142) have quartz-calcite thermometers that were able to limit the pressure conditions from the isochors (shown by the stars in Fig. 14). The pressure range for AR96 is 1.6 - 2.5 kbars (6-10 km) and the pressure range of AR142 is 2.4 - 3.0 kbars (9 - 12 km) using the quartz-calcite temperatures calculated from Sharp and Kirschner, (1994). The average pressure range for AR96 is 2.2 kbars (8 km) and 2.7 kbars (11 km) for AR142. The quartz-calcite temperatures calculated using Clayton et al. (1989) are low, and suggest formation pressures of zero kbars.

The depths for these pressures were calculated using $P = \rho g z$ where P is pressure (N), ρ is saturated rock density taken as 2.65×10^3 kg·m^{-3}, g is the acceleration due to gravity (m/s^2), and z is depth (m). To use this equation we assume a lithostatic geothermal gradient (Fig. 15 shows an average lithostatic geothermal gradient of

~30ºC/km). This value was determined by using the quartz-calcite fractionation temperatures and temperatures calculated from Sharp and Kirschner, (1994) to constrain the average isochore for each sample.

For samples without quartz-calcite thermometry, vitrinite reflectance (Ro) was plotted in conjunction with the isochores to constrain the maximum pressure of vein formation (solid boxes in Fig. 14). For all samples plotted in Figure 14, the temperatures calculated from Ro ranged from 265º - 376ºC, which falls within the range calculated from quartz-calcite isotope thermometry using the equation of Sharp and Kirschner (1994). This temperature range can be converted to depth ranges assuming different geothermal gradients. Using a geothermal gradient of 35°C/km we get depths of 7 - 11 km, using a geothermal gradient of 25°C/km we get depths of 10 - 15 km, and using a geothermal gradient of 15°C/km we get depths of 17 - 25 km (Fig 16). When temperatures are constrained to pre-Carboniferous strata (using Ro values of Houseknecht and Matthews, 1985), the depths and temperatures increase slightly, as shown by the shaded box in Figure 16.

We also used the Ro temperature to constrain the average isochore of each sample and obtain an average pressure range of vein formation for each sample. These pressures (0.3 – 4.7 kbars) were then converted to depths of vein formation (0 – 19 km) using $P = \rho gz$, as was done for the samples with quartz-calcite temperatures. The ranges of Ro, pressure and depth of each sample seen in Figure 14 are reported in Table 4. These depths of vein emplacement are plotted on the depth of burial curves in Figure 17

as bold lines. The calculated depths (via pressure) overlap, indicating an early to middle Pennsylvanian period of emplacement.

6. DISCUSSION

6.1. Assumptions and Problems

The results of this study are dependant on a handful of key assumptions in both the geology and in the methodology used. First, the veins must be cogenetic. A key assumption for proper interpretation of the temperatures derived from quartz-calcite isotope thermometry is that both mineral phases co-precipitate from the same fluid. We assume that there has been no post-precipitation or alteration of the isotopic compositions. Calcite recrystallization is possible, although the existence of twinning in calcite means that any recrystallization is pre- or syn-tectonic. Our evidence for co-precipitation are textural observations from thin sections and XRF element scans. The fact that the $1000\ln\alpha$ values for most quartz-calcite minerals pairs are also positive supports, but does not prove, the conclusion.

The choice of quartz-calcite fractionation equations also makes a large difference in calculated temperature. There is also a large discrepancy between the Clayton et al. (1989) and Sharp and Kirschner (1994) temperature estimates. The temperatures derived from Clayton et al. (1989) are lower than previous thermal estimates and yield vein formation pressures of zero kbars. These temperatures and pressures do not agree with previous work but can be accurate if veins formed at the surface. The Sharp and Kirschner (1994) method yields temperatures most consistent with our results, previous thermal estimates and the degree of metamorphism observed in the field. We have

reported both temperature ranges up to this point, but will now use the temperatures of Sharp and Kirschner (1994) for reasons stated above.

6.2. Fluid Flow

Stable isotope analysis provides a key to understanding fluid flow and source, and thus the mode of transport for vein-forming material. Isotopic variability between host and vein material is an important indication of whether the vein-forming fluid was in equilibrium with the host or if the vein-forming fluid was allochthonous.

Similar isotopic values between the vein and host suggest that the vein-forming fluid was is in isotopic equilibrium with the host, where local fluid diffused from the host pore fluid into the vein precipitation sites (e.g. Durney and Ramsay, 1973; Fisher and Brantley, 1992). Isotopic differences of 2 - 4‰ between vein and host rocks has been interpreted by many workers to be indicative of equilibrium formation (e.g., Cartwright et al., 1994; Al-Aasm et al., 1995; Kirschner et al., 1995; Henry et al., 1996; Kenis et al., 2000; Ghisetti et al., 2001, Richards et al., 2002; Hilgers and Urai, 2002). For example, vein and host quartz $\delta^{18}O$ values within 2‰ from the Ormiston Gorge in Australia led Cartwright et al. (1994) to suggest vein-host equilibrium. Similarly, Kirschner et al. (1995) found quartz-calcite veins from the Morcles Nappe in the Swiss Alps to have $\delta^{18}O$ and $\delta^{13}C$ vein-host similarities within 3‰. Also, Ghisetti et al. (2001) report veins from the central Apennines in Italy to have vein-host $\delta^{18}O$ isotopic similarities within 4‰.

When a vein and host have dissimilar isotopic values, the fluid is considered not to have formed in equilibrium with the host and may have traveled some distance through available fluid flow paths (fractures, bulk permeability; e.g. Etheridge et al., 1983; Rye and Bradbury, 1988; Walther, 1990; Stueber and Walter, 1991; Ferry and Dipple, 1991). Allochthonous fluids cause large isotopic variations between host and vein material as reported by several workers (e.g., Dietrich et al., 1983; Rye and Bradbury, 1988; Shemesh et al., 1992; Kirschner et al., 1993; Hilgers and Urai, 2002). For example, vein and host differences of 3.1‰ in calcite $\delta^{18}O$ from a thrust fault zone in the Pyrenees led Rye and Bradbury (1988) to conclude that the veins were formed from openly circulating fluids. Differences in host and vein quartz $\delta^{18}O$ of 7‰ from the Morcles Nappe in the Swiss Alps led Kirschner et al. (1993) to suggest that vein forming fluid traveled through faults. Similarly, Hilgers and Urai (2002) attributed vein and host differences up to 9‰ in calcite $\delta^{18}O$ to late forming veins in which the fluid was infiltrated through normal faults.

Previous work from Ouachita veins near Hot Springs Village, AK show quartz vein-host $\delta^{18}O$ differences within 2‰, which suggests that vein forming fluid evolved from local and rock-buffered to a short traveled fluid (Cervantes and Wiltschko, 2010). For our veins, the average isotopic variation between vein and host $\delta^{18}O$ is 2.4 ± 1.7‰. The small isotopic differences in vein-host quartz $\delta^{18}O$ values and the host dominated isotopic composition in our veins suggest that the vein-forming fluid was at or near isotopic equilibrium with the host.

The small isotopic variation between host and vein is also observed in calcite $\delta^{18}O$ and $\delta^{13}C$, with average differences of 0.7 ± 1.7‰ and 0.4 ± 1.6‰ for oxygen and carbon, respectively, for all of the data (Table 2). The difference in vein and host calcite $\delta^{18}O$ ranges from -3.9 - 7.3‰ and is equivalent to a temperature range of ~70ºC, assuming a fluid composition of 19.0 - 30.6‰ (VSMOW) for the Ordovician through Carboniferous (e.g. Veizer et al., 1999; Buggisch et al., 2008; Grossman et al., 2008).

6.3. Vein Emplacement

Syntectonic veins are considered to be late Pennsylvanian to early Permian, as discussed in section 2.4. This age is further supported by burial curves for selected formations (Fig. 17). Average structural thicknesses from the Ouachita core were used to estimate the stratigraphic depth of each formation. It is not known if these thicknesses are true stratigraphic thicknesses or if structural thickening has occurred. The depths of vein formation (shown as bolded lines on Fig. 17) were calculated using Ro temperature constraints on the average isochore of each sample. The burial curves allow us to constrain the timing of vein emplacement based on when the formation burial curves coincide with the calculated depths of vein formation. The timing we get from Figure 17 is early to middle Pennsylvanian, which agrees with previous studies (e.g. Bass and Ferrara, 1969; Shelton et al., 1986).

If these veins are syntectonic, then they could be related to early Permian heating seen in the AFT thermal history model of Winkler et al. (1999; Fig. 6). The temperatures

of vein formation we calculated are well above the partial annealing zone and are in agreement with the AFT model, which shows that the grains were reset at this time.

Vein formation conditions correspond to lithostatic geothermal gradients of ~20º - 50ºC/km, with an average of ~30ºC/km (Fig. 20). These values were found by using the temperatures calculated from Sharp and Kirschner, (1994) to constrain the average isochore for each sample. We then overlaid various lithostatic and hydrostatic gradients on the isochors to evaluate which best fit the data. One exception to the trend of lithostatic vein formation pressures is AR119. This sample corresponds to an average hydrostatic geothermal gradient of ~35ºC/km as is represented by the small shaded box in Figure 20. The reason for this outlier is unknown, but this sample is the farthest north of all the samples and lies outside of the Ouachita core, in the youngest and coldest Ouachita strata.

7. CONCLUSIONS

1) The appearance of interdigitated quartz and calcite grains in both thin section and XRF images supports equilibrium growth. Therefore, one of the essential prerequisites for using the quartz-calcite thermometer in the core of the Ouachita orogen is satisfied. In addition, the veins are pre- or syntectonic because they contain twinned calcite grains.

2) The small differences in vein-host isotopic values and the host dominated isotopic composition in our veins suggest that the vein-forming fluid was at or near isotopic equilibrium with the host.

3) Using only positive quartz-calcite fractionations, the temperature of formation for veins ranges from 211° - 429°C (using equation of Sharp and Kirschner, 1994).

4) $\delta^{18}O$ and $\delta^{13}C$ isotopic values in vein and host quartz and calcite do not significantly vary regionally or stratigraphically.

5) Vein formation temperatures calculated from quartz-calcite fractionations are similar in all of the formations , suggesting veins are from the same or slightly changing fluid source.

6) Fluid inclusion homogenization temperatures range from 106º - 285ºC with an average of 176º ± 40ºC. The average homogenization temperature slightly increases to the east.

7) The maximum temperature calculated using vitrinite reflectance (Ro) is 265º - 376ºC. This is within the range of vein formation temperatures calculated using Sharp

and Kirschner, (1994) equation for quartz-calcite isotope thermometry. This Ro temperature range is equivalent to depths of 10 - 15 km using a geothermal gradient of 25°C/km.

8) The pressure of vein formation from fluid inclusion isochores constrained by quartz-calcite fractionation and vitrinite reflectance temperatures is 1.6 – 3.0 kbars and 0.3 – 4.7 kbars, respectively. These pressures correspond to depths of 6 – 12 km and 0 - 19 km, respectively, using $P = \rho gz$. Veins formation pressures correspond to an average lithostatic geothermal gradient of ~30ºC/km.

9) The timing of vein emplacement appears to be early to middle Pennsylvanian based on reconstructed depths of vein formation compared to burial history.

REFERENCES

Al-Aasm, I.S., Coniglio, M., Desrochers, A., 1995. Formation of complex fibrous calcite veins in Upper Triassic strata of Wrangellia Terrain, British Columbia, Canada. Sedimentary Geology 100, 83-95.

Arbenz, J.K., 1989. The Ouachita system. In: Bally, A.W. and Palmer, A.R. (Eds.), The Geology of North America - an overview A, Geological Society of North America, Boulder, Colorado, 371-396.

Arne, D.C., 1992. Evidence from apatite fission-track analysis for regional Cretaceous cooling in the Ouachita mountain fold belt and Arkoma basin of Arkansas. American Association of Petroleum Geologists Bulletin 76, 392-402.

Bass, M.N., Ferrara, G., 1969. Age of adularia and metamorphism, Ouachita Mountains, Arkansas. American Journal of Science 267, 491-498.

Blackmer, G., Omar, G.I., Gold, D.P., 1994. Post-Alleghanian unroofing history of the Appalachian basin, Pennsylvania, from apatite fission track analysis and thermal models. Tectonics 13, 1259-1276.

Briggs, G., Roeder, D., 1978. Sedimentation and plate tectonics, Ouachita mountains and Arkoma basin. In: Chamberlain, C. K., (Ed.), A guidebook to the trace fossils and paleoecology of the Ouachita Geosyncline. Society of Economic Paleontologists and Mineralogists, Tulsa, 1-22.

Buggisch, W., Joachimski, M.M., Sevastopulo, G., Morrow, J.R., 2008. Mississippian $\delta^{13}C_{carb}$ and conodont apatite $\delta^{18}O$ records - Their relation to the late Paleozoic Glaciation. Palaeogeography, Palaeoclimatology, Palaeoecology 268, 273-292.

Burtner, R.L., Nigrini, A., Donelick, R.A., 1994. Thermochronology of lower Cretaceous source rocks in the Idaho-Wyoming Thrust Belt. American Association of Petroleum Geologists Bulletin 78, 1613-1636.

Byrnes, A., Lawyer, G., 1999. Burial, maturation, and petroleum generation history of the Arkoma Basin and Ouachita Foldbelt, Oklahoma and Arkansas. Natural Resources Research 8, 3-26.

Cartwright, I., Power, W.L., Oliver, N.H.S., Valenta, R.K., McLatchie, G.S., 1994. Fluid migration and vein formation during deformation and greenschist facies metamorphism at Ormiston Gorge, central Australia. Journal of Metamorphic Geology 12, 373-386.

Cebull, S.E., Shurbet, D.H., Keller, G.R., Russell, L.R., 1976. Possible role of transform faults in the development of apparent offsets in the Ouachita-southern Appalachian tectonic belt. The Journal of Geology 84, 107-114.

Cervantes, P., Wiltschko, D.V., 2010. Tip to midpoint observations on syntectonic veins, Ouachita orogen, Arkansas: Trading space for time. Journal of Structural Geology 32, 1085-1100.

Clayton, R., Goldsmith, J.R., Mayeda, T.K., 1989. Oxygen isotope fractionation in quartz, albite, anorthite and calcite. Geochimica et Cosmochimica Acta 53, 725-733.

Clayton, R., Mayeda, T.K., 1963. The use of bromine pentafluoride in the extraction of oxygen from oxides and silicates for isotopic analysis. Geochimica et Cosmochimica Acta 27, 43-52.

Corrigan, J., Cervany, P.F., Donelick, R., Bergman, S.C., 1998. Postorogenic denudation along the late Paleozoic Ouachita trend, south central United States of America magnitude and timing constraints from apatite fission track data. Tectonics 17, 587-603.

Curtis, D.M., 1991. The northern Gulf of Mexico basin. In: Gluskoter, H. J.; Rice, D. D.; Taylor, R. B. (Eds.), Economic Geology, U.S. – The geology of North America. Geologic Society of America, Boulder, Colorado, 301-324.

Dickinson, W., 1974. Plate tectonics and sedimentation. Special publication - Society of Economic Paleontologists and Mineralogists 22, 1-27.

Dietrich, D., MacKenzie, J.A., Song, H., 1983. Origin of calcite in syntectonic veins as determined from carbon-isotope ratios. Geology 11, 547-551.

Dow, W.G., 1977. Kerogen studies and geological interpretations. Journal of Geochemical Exploration 7, 79-99.

Durney, D.W., Ramsey, J.G., 1973. Incremental strains measured by syntectonic crystal growths. In: De Jong, K.A., Scholten. R. (Eds.), Gravity and Tectonics. Wiley, New York, 67-96.

Engel A.E.J., 1952. Quartz crystal deposits of western Arkansas. U. S. Geological Survey Bulletin, 973E, 173-260.

Etheridge, M.A., Wall, V.J., Vernon, R.H., 1983. The role of the fluid phase during regional metamorphism and deformation. Journal of Metamorphic Geology 1, 205-226.

Ethington, R.L., Finney, S.C., Repetski, J.E., 1989. Biostratigraphy of the Paleozoic rocks of the Ouachita Orogen, Arkansas, Oklahoma, West Texas. In: Hatcher, R.D., Jr.; Thomas, W.A.; Viele, G.W. (Eds.), The Appalachian-Ouachita Orogen in the United States. DNAG, the Geology of North America F-2. Geological Society of America, Boulder, Colorado, 563-574.

Ferry, J., Dipple, G.M., 1991. Fluid flow, mineral reactions, and metasomatism. Geology 19, 211-214.

Fisher. D., Brantley, S.L., 1992. Models of quartz overgrowth and vein formation deformation and episodic fluid flow in an ancient subduction zone. Journal of Geophysical Research 97, 20043-20061.

Fuller, C.W., Willett, S.D., Fisher, D., Lu, C.Y., 2006. A thermomechanical wedge model of Taiwan constrained by fission-track thermochronometry. Tectonophysics 425, 1-24.

Ghisetti, F., Kirschner, D.L., Vezzani, L., Agosta, F., 2001. Stable isotope evidence for contrasting paleofluid circulation in thrust faults and normal faults of the Central Apennines, Italy. Journal of Geophysical Research 106, 8811-8825.

Goldstein, A., Jr., Reno, D.H., 1952. Petrography and metamorphism of sediments of Ouachita facies. American Association of Petroleum Geologists Bulletin 36, 2275-2290.

Graham, S.A., Dickinson, W.R., Ingersoll, R.V., 1975. Himalayan-Bengal model for flysch dispersal in the Appalachian-Ouachita system. Geological Society of America Bulletin 86, 273-286.

Grossman, E., 2008. Glaciation, aridification, and carbon sequestration in the Permo-Carboniferous the isotopic record from low latitudes. Palaeogeography, Palaeoclimatology, Palaeoecology 268, 222.

Guthrie, J., Houseknecht, D.W., Johns, W.D., 1986. Relationships among vitrinite reflectance, illite crystallinity, and organic geochemistry in Carboniferous strata, Ouachita Mountains, Oklahoma and Arkansas. American Association of Petroleum Geologists Bulletin 70, 26-33.

Haley, B.R., Stone, C.G., 1996. CoGeo Maps of Arkansas. Arkansas Geological Commission, Little Rock, Arkansas.

Helsen, S., David, P., Fermont, W.J.J., 1995. Calibration of conodont color alteration using color image analysis. The Journal of Geology 103, 257-267.

Henry, C., Burkhard, M., Goffe, B., 1996. Evolution of synmetamorphic veins and their wallrocks through a Western Alps transect no evidence for large-scale fluid flow stable isotope, major- and trace-element systematics. Chemical Geology 127, 81-109.

Heroux, Y., Chagnon, A., Bertrand, R., 1979. Compilation and correlation of major thermal maturation indicators. The American Association of Petroleum Geologists Bulletin 63, 2128-2144.

Hildenbrand, T.G., Kane, M.F., Hendricks, J.D., 1982. Magnetic basement in the upper Mississippi Embayment region a preliminary report. U. S. Geological Survey Professional Paper, P1236, 39-53.

Hilgers, C., Urai, J.L., 2002. Microstructural observations of natural syntectonic fibrous veins: Implications for the growth process. Tectonophysics 352, 257-264.

Honess, C.W., 1923. Geology of the southern Ouachita Mountains of Oklahoma. Oklahoma Geological Survey Bulletin 32, 278p.

Houseknecht, D., Matthews, S.M., 1985. Thermal maturity of Carboniferous strata, Ouachita Mountains. American Association of Petroleum Geologists Bulletin 69, 335-345.

Johnson, K., Amsden, T.W., Denison, R.E., Dutton, S.P., Goldstein, A.G., Rascoe, B., Jr., Sutherland, P.K., Thompson, D.M., 1988. Southern midcontinent region. In: Sloss, L.L. (Ed.), Sedimentary Cover; North American Craton; U.S. DNAG, the Geology of North America D-2. Geological Society of America, Boulder, Colorado, 307-359.

Keller, G.R., Cebull, S.E., 1973. Plate tectonics and the Ouachita system in Texas, Oklahoma, and Arkansas. Geological Society of America Bulletin 84, 1659-1665.

Keller, W., Stone, C.G., Hoersch, A.L., 1985. Textures of Paleozoic chert and novaculite in the Ouachita Mountains of Arkansas and Oklahoma and their geological significance. Geological Society of America Bulletin 96, 1353-1363.

Kenis, I., Muchez, P., Sintubin, M., Mansy, J.L., Lacquement, F., 2000. The use of a combined structural, stable isotope and fluid inclusion study to constrain the

kinematic history at the northern Variscan front zone (Bettrechies, northern France). Journal of Structural Geology 22, 589-602.

Kirschner, D., Sharp, Z.D., Masson, H., 1995. Oxygen isotope thermometry of quartz-calcite veins unraveling the thermal-tectonic history of the subgreenschist facies Morcles Nappe (Swiss Alps). Geological Society of America Bulletin 107, 1145-1156.

Kirschner, D.L., Sharp, Z.D., Teyssier, C., 1993. Vein growth mechanisms and fluid sources revealed by oxygen isotope laser microprobe. Geology 21, 85-88.

Konig, R., Stone, C.G., 1977. Geology of abandoned Kellogg lead-zinc-silver-copper mines, Pulaski County, Arkansas. In: Stone, C.G.; Haley, B.R.; Holbrook, D.F.; Williams, N.F.; Bush, W.V.; McFarland, J.D. (Eds.), Symposium on the geology of the Ouachita Mountains; Volume II, Economic geology, mineralogy, and miscellaneous. Arkansas Geologic Commission, Little Rock, Arkansas, 14, 5-17.

Kruger, J.M., Keller, G.R., 1986. Interpretation of crustal structure from regional gravity anomalies, Ouachita Mountains area and adjacent Gulf Coastal Plain. American Association of Petroleum Geologists Bulletin 70, 667-689.

Lillie, R.J., Nelson, K.D., de Voogd, B., Brewer, J.A., Oliver, J.E., Brown, L.D., Kaufman, S., Viele, G.W., 1983. Crustal structure of Ouachita Mountains, Arkansas a model based on integration of COCORP reflection profiles and regional geophysical data. American Association of Petroleum Geologists Bulletin 67, 907-931.

Lowe, D., 1989. Stratigraphy, sedimentology, and depositional setting of pre-orogenic rocks of the Ouachita Mountains, Arkansas and Oklahoma. In: Hatcher, R.D., Jr.; Thomas, W.A.; Viele, G.W. (Eds.), The Appalachian-Ouachita Orogen in the United States. DNAG, the Geology of North America F-2. Geological Society of America, Boulder, Colorado, 575-590.

Mao, S., Duan, Z., 2008. The P,V,T,*x* properties of binary aqueous chloride solutions up to T = 573 K and 100 MPa. Journal of Chemical Thermodynamics 40, 1046-1063.

McBride, E.F., 1975. The Ouachita trough sequence Marathon region and Ouachita Mountains. In: Briggs, G.; McBride, E.F.; Moiola, R.J. (Eds.), A guidebook to the sedimentology of Paleozoic flysch and associated deposits, Ouachita Mountains; Arkoma Basin, Oklahoma. Dallas Geologic Society, Dallas, Texas, 23-41.

Miser, H., 1943. Quartz veins in the Ouachita Mountains of Arkansas and Oklahoma, their relations to structure, metamorphism, and metalliferous deposits. Economic Geology and the Bulletin of the Society of Economic Geologists 38, 91-118.

Miser, H., 1959. Structure and vein quartz of the Ouachita Mountains of Arkansas and Oklahoma. In: Cline, L.M.; Hilsewick, W.J.; Feray, D.E. (Eds.), Ouachita Symposium. Dallas and Ardmore Geological Societies, Dallas, Texas, 30-43.

Morris, R., 1989. Stratigraphy and sedimentary history of post-Arkansas Novaculite Carboniferous rocks of the Ouachita Mountains. In: Hatcher, R.D., Jr.; Thomas, W.A.; Viele, G.W. (Eds.), The Appalachian-Ouachita Orogen in the United States. DNAG, the Geology of North America F-2. Geological Society of America, Boulder, Colorado, 591-602.

Naeser, C., Naeser, N.D., Southworth, S., 2006. Tracking across the Southern Appalachians eastern Tennessee and western Carolinas. Abstracts with programs - Geological Society of America 38, p.67.

Nelson, K.D., Lillie, R.J., de Voogd, B., Brewer, J.A., Oliver, J.E., Kaufman, S., Brown, L., Viele, G.W., 1982. COCORP seismic reflection profiling in the Ouachita Mountains of western Arkansas; Geometry and geologic interpretation. Tectonics 1, 413-430.

Nielsen, K.C., Viele, G.W., Zimmerman, J., 1989. Structural setting of the Benton-Broken Bow uplifts. In: Hatcher, R.D., Jr.; Thomas, W.A.; Viele, G.W. (Eds.), The Appalachian-Ouachita Orogen in the United States. DNAG, the Geology of North America F-2. Geological Society of America, Boulder, Colorado , 635-660.

O'Neil, J., 1986. Theoretical and experimental aspects of isotopic fractionation. Reviews in Mineralogy 16, 1-40.

Poole, F., Perry, W.J., Jr., Madrid, P., Amaya-Martinez, R., 2005. Tectonic synthesis of the Ouachita-Marathon-Sonora orogenic margin of southern Laurentia: Stratigraphic and structural implications for timing of deformational events and plate tectonic model. In: Anderson, T.H.; Nourse, J.A.; McKee, J.W.; Steiner, M.B. (Eds.), The Mojave-Sonora megashear hypothesis: Development, assessment, and alternatives. Geological Society of America Special Paper 393, Geological Society of America, Boulder, Colorado, 543-596.

Price, L.C., 1983. Geologic time as a parameter in organic metamorphism and vitrinite reflectance as an absolute paleogeothermometer. Journal of Petroleum Geology 6, 5-38.

Rejebian, V., Harris, A.G., Huebner, J.S., 1987. Conodont color and textural alteration an index to regional metamorphism, contact metamorphism, and hydrothermal alteration. Geological Society of America Bulletin 99, 471-479.

Richards, I., Connelly, J.B., Gregory, R.T., Gray, D.R., 2002. The importance of diffusion, advection, and host-rock lithology on vein formation a stable isotope study from the Paleozoic Ouachita orogenic belt, Arkansas and Oklahoma. Geological Society of America Bulletin 114, 1343-1355.

Roden, M., Miller, D.S., 1989. Apatite fission-track thermochronology of the Pennsylvania Appalachian Basin. Geomorphology 2, 39-51.

Roden, M.K., 1991. Apatite fission-track thermochronology of the southern Appalachian Basin; Maryland, West Virginia, and Virginia. The Journal of Geology 99, 41-53.

Roedder, E., 1984. Fluid inclusions. In: Roedder, E. (Ed.), Reviews in Mineralogy 12. Mineralogical Society of America, Washington, D.C., 71-77.

Rye, D., Bradbury, H.J., 1988. Fluid flow in the crust an example from a Pyrenean thrust ramp. American Journal of Science 288, 197-235.

Sharp, Z.D., Kirschner, D.L., 1994. Quartz-calcite oxygen isotope thermometry: A calibration based on natural isotopic variations. Geochimica et Cosmochimica Acta 58, 4491-4501.

Sharp, Z.D., 2007. Principles of Stable Isotope Geochemistry. Pearson Prentice Hall, Upper Saddle River, New Jersey, 40-63.

Shelton, K., Reader, J.M., Ross, L.M., Viele, G.W., Seidemann, D.E., 1986. Ba-rich adularia from the Ouachita Mountains, Arkansas; Implications for a postcollisional hydrothermal system. The American Mineralogist 71, 916-923.

Shemesh, A., Ron, H., Erel, Y., Kolodny, Y., Nur, A., 1992. Isotopic composition of vein calcite and its fluid inclusions; Implication to paleohydrological systems, tectonic events and vein formation processes. Chemical Geology; Isotope Geoscience Section 94, 307-314.

Stewart, J.H., 1976. Late Precambrian evolution of North America; Plate tectonics implication. Geology 4, 11-15.

Stone, C., Haley, B.R., 1994. Quartz veins and crystal deposits in the Ouachita Mountains. Abstracts with programs - Geological Society of America 26, p.28.

Stone, C.G., McFarland, J.D., III, Haley, B.R., 1982. Field guide to the Paleozoic rocks of the Ouachita Mountain and Arkansas Valley provinces, Arkansas. In: Stone, C.G.; McFarland, J.D., III; Haley, B.R. (Eds.), Guidebook - Arkansas Geological Commission 81-1. Arkansas Geological Commission, Little Rock, Arkansas, 140p.

Stueber, A., Walter, L.M., 1991. Origin and chemical evolution of formation waters from Silurian-Devonian strata in the Illinois Basin, USA. Geochimica et Cosmochimica Acta 55, 309-325.

Thomas, W., 1991. The Appalachian-Ouachita rifted margin of southeastern North America. Geological Society of America Bulletin 103, 415-431.

Thomas, W.A., 1976. Evolution of Ouachita-Appalachian continental margin. The Journal of Geology 84, 323-342.

Thomas, W.A., 1977. Evolution of Appalachian-Ouachita salients and recesses from reentrants and promontories in the continental margin. American Journal of Science 277, 1233-1278.

Veizer J., Ala, D., Azmy, K., Bruckschen, P., Buhl, D., Bruhn, F., Carden, G.A.F., Diener, A., Ebneth, S., Godderis, Y., Jasper, T., Korte, C., Pawellek, F., Podlaha, O.G., Strauss, H., 1999. $^{87}Sr/^{86}Sr$, $\delta^{13}C$ and $\delta^{18}O$ evolution of Phanerozoic seawater. Chemical Geology 161, 59-88.

Viele, G.W., Thomas, W.A., 1989. Tectonic synthesis of the Ouachita orogenic belt. In: Hatcher, R.D., Jr.; Thomas, W.A.; Viele, G.W. (Eds.), The Appalachian-Ouachita Orogen in the United States. DNAG, the Geology of North America F-2. Geological Society of America, Boulder, Colorado, 695-728.

Walther, J., 1990. Fluid dynamics during progressive regional metamorphism. Studies in geophysics, the role of fluids in crustal processes. American Geophysical Union Symposium. National Academic Press, Washington, DC, 64-71.

Werre, R.W., Bodnar, R.J., Bethke, P.M., Barton, P.B., Jr., 1979. A novel gas-flow inclusion heating/freezing stage. Abstracts with Programs – Geological Society of America 11, p.539.

Whitaker, A., Engelder, T., 2006. Plate-scale stress fields driving the tectonic evolution of the central Ouachita Salient, Oklahoma and Arkansas. Geological Society of America Bulletin 118, 710-723.

Winkler, J., Kelley, S.A., Bergman, S.C., 1999. Cenozoic denudation of the Wichita Mountains, Oklahoma, and southern Mid-continent apatite fission-track thermochronology constraints. In: Marshak, S.; van der Pluijm, B.A.; Hamburger, M. (Eds.), Tectonics of Continental Interiors. Geological Society of America, Penrose Conference on Tectonics of Continental Interiors. Elsevier, Amsterdam, The Netherlands, Tectonophysics 305, 339-353.

Zheng, Y., 1993. Calculation of oxygen isotope fractionation in anhydrous silicate minerals. Geochimica et Cosmochimica Acta 57, 1079-1091.

Zhenhao Duan Research Group, 2011. Fluid inclusion modeling software. http://calc.geochem-model.org/Pages/H2ONaCl.aspx. Institute of Geology and Geophysics, Chinese Academy of Sciences. Access date: July 10, 2011.

APPENDIX A

FIGURES

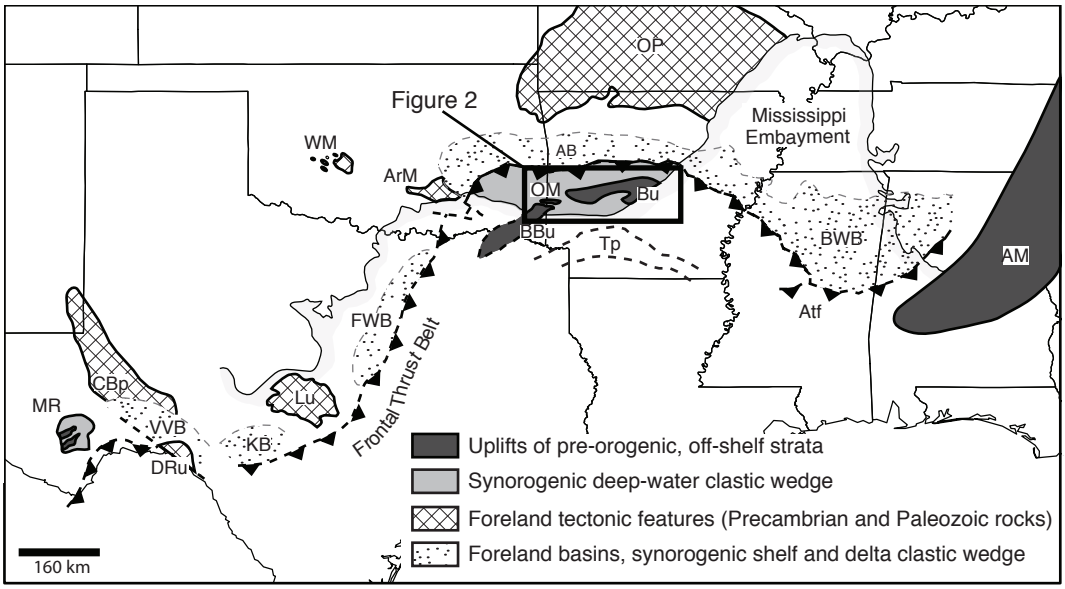

Fig. 1: Index map of the Ouachita-Marathon collision belt (OMCB) and adjacent areas (after Arbenz, 1989; and Viele and Thomas, 1989). AB, Arkoma Basin; AM, Appalachian Mountains; ArM, Arbuckle Mountains; Atf, Appalachian tectonic front; BBu, Broken Bow uplift; Bu, Benton uplift; BWB, Black Warrior Basin; CBp, Central Basin platform; DRu, Devils River uplift; FWB, Fort Worth Basin; KB, Kerr Basin; Lu, Llano uplift; MR, Marathon Region; OM, Ouachita Mountains; OP, Ozark Plateau; Tp, Texarkana platform; VVB, Val Verde Basin; WM, Wichita Mountains. Inset box shows the location of Figure 2.

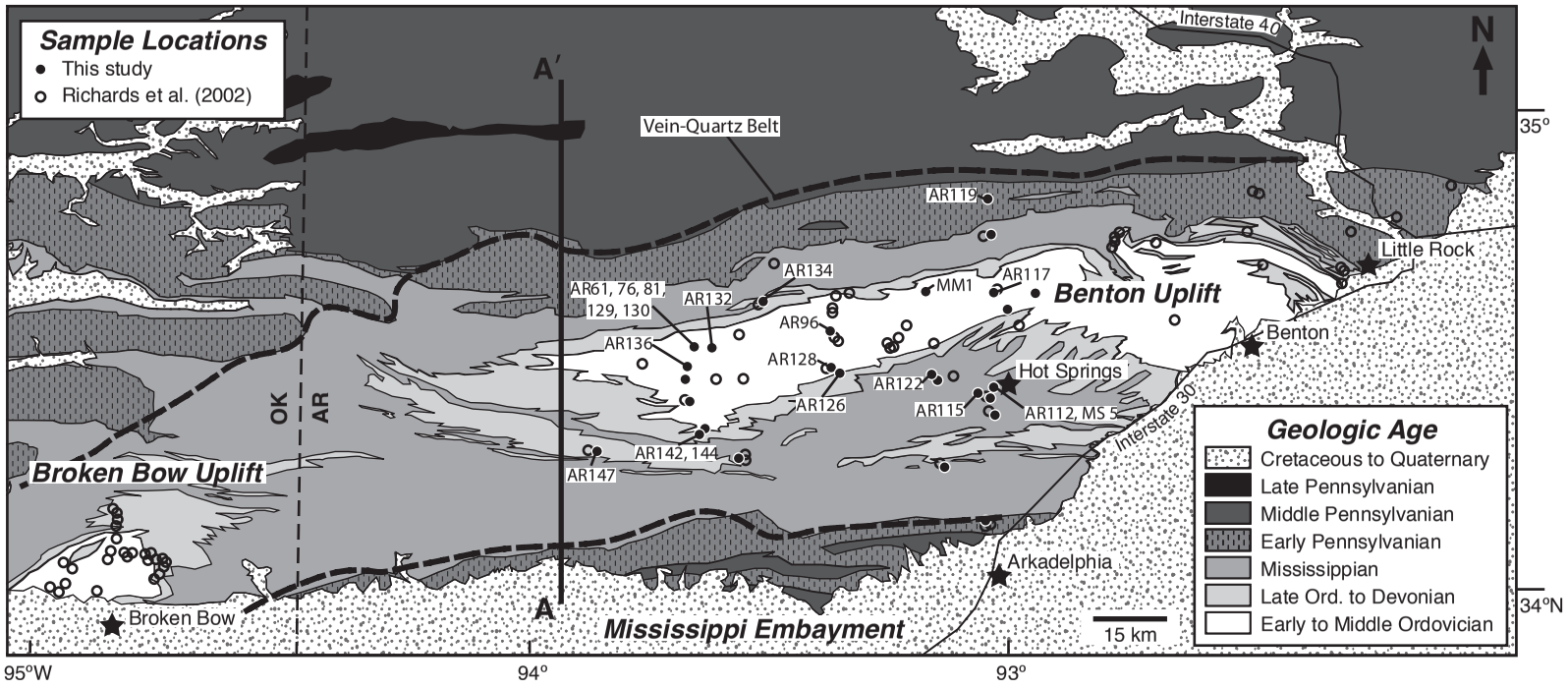

Fig. 2: Geologic map of the Ouachita Mountains, after United States Geological Survey digital maps of Arkansas and Oklahoma showing the location of samples used for isotopic study. The approximate location of the vein-quartz belt is shown by the bold dashed line (e.g. Miser, 1943, 1959; Richards et al., 2002). Approximate latitude and longitude shown for samples of Richards et al. (2002). Line A-A' is the location of the cross-section in Figure 3.

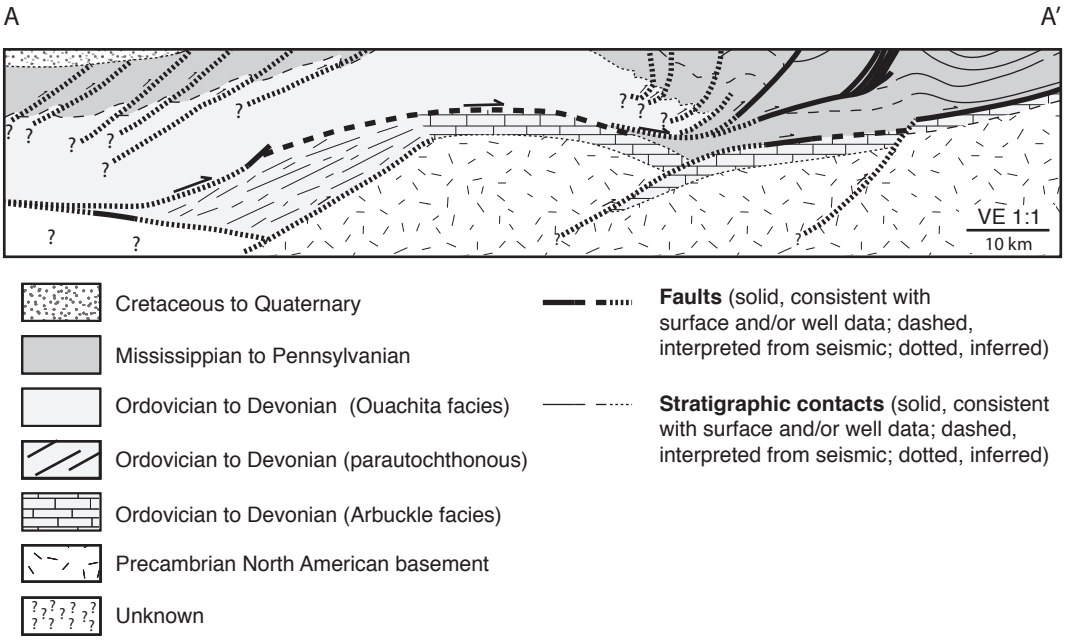

Fig. 3: Geologic interpretation of the COCORP seismic reflection profile along A-A', Fig. 2, after Nelson et al. (1982) and Lillie et al. (1983). The cross-section shows roughly the upper 25 kilometers of crust and is approximately 1:1 assuming an average upper crustal velocity of 5 kilometers per second.

Age (Ma)	Period	Formation	Thickness (m)	Cum. Thick. (km)	Lithology	
300	Carboniferous: Pennsylvanian					SYNOROGENIC
		Atoka Fm. (Pa)	5700-8613	5.70-8.61	Shale, sandstone.	
		Johns Valley Sh. (Pjv)	429-484	6.13-9.10	Shale, sandstone, limestone.	
		Jackfork Ss. (Pj)	1678-2100	7.81-11.20	Sandstone, shale.	
	Carboniferous: Mississippian	Stanley Sh. (Ms)	3234-3600	11.04-14.80	Shale, siltstone, sandstone, tuff.	
350					Upper: Chert, novaculite, shale.	PREOROGENIC
	Devonian	Arkansas Novaculite (MDa)	200-297	11.24-15.09	Middle: Chert, novaculite, shale, conglomerate.	
400					Lower: Novaculite, shale, conglomerate.	
	Silurian	Missouri Mtn. Sh. (Smb)	15-91	11.26-15.19	Shale, chert, quartzose sandstone.	
		Blaylock Ss. (Smb)	67-457	11.32-15.64	Sandstone, shaly siltstone, shale.	
	Ordovician	Polk Creek Sh. (Opb)	12-53	11.34-15.70	Shale, chert, limestone.	
450		Bigfork Chert (Opb)	200-285	11.54-15.98	Chert, shale, limestone.	
		Womble Sh. (Ow)	264-1050	11.80-17.03	Shale, limestone, siltstone, minor quartzose sandstone.	
		Blakely Ss. (Ob)	120-165	11.92-17.20	Shale, quartzose sanstone.	
		Mazarn Sh. (Om)	875-957	12.79-18.15	Shale, thin sandstone, limestone.	
		Crystal Mtn. Ss. (Ocm)	125-297	12.92-18.45	Massive calcareous to quartzitic sandstone.	
500		Collier Sh. (Oc)	264-475	13.18-18.92	Shale, siliceous limestone, chert.	

Fig. 4: Stratigraphic column of the Ouachita Mountains (after Richards et al., 2002 with dates from Ethington et al., 1989). Stratigraphic thicknesses are from Briggs et al. (1975), Thomas (1976), Stone et al. (1982), Arbenz (1989), and Viele and Thomas (1989). Grey shading corresponds to the shading used in Figure 3. Column labeled "Cum. thick" is the cumulative stratigraphic thickness measured from the youngest exposed rocks toward increasing age and stratigraphic depth.

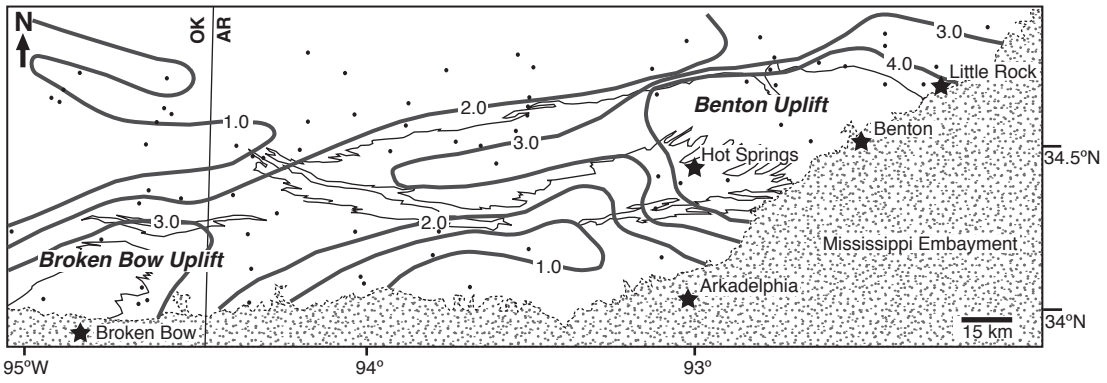

Fig. 5: Contoured vitrinite reflectance map of the Ouachita Orogen (modified after Houseknectht and Mathews, 1985). Small dots are sample localities of Houseknectht and Mathews (1985). The shaded region is the Cretaceous to Quaternary onlap. The thin lines are the approximate location of the Devonian - Mississippian contact.

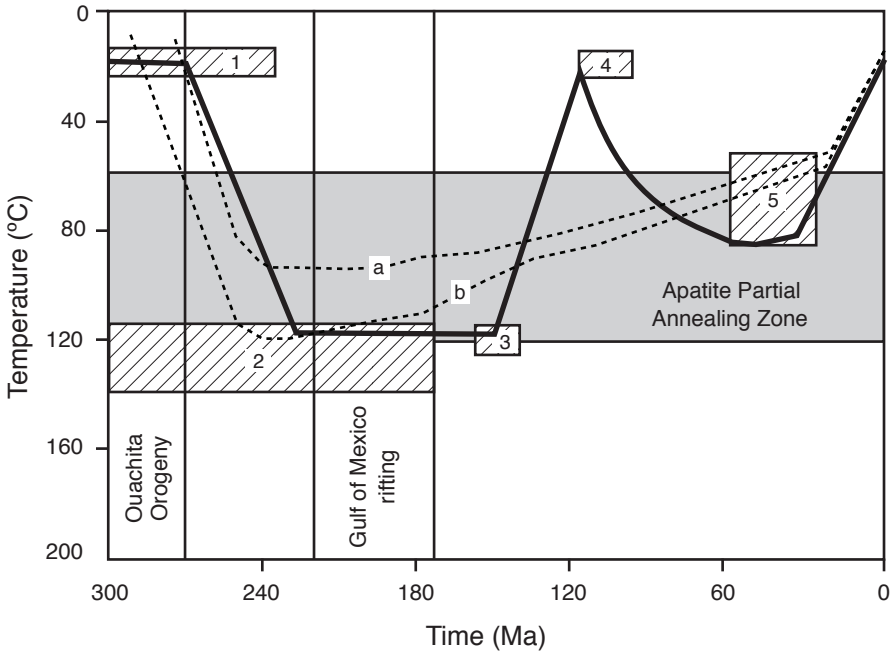

Fig. 6: Regional thermal model for the Ouachita orogen and surrounding areas based on AFT data (modified from Winkler et al., 1999). The timing of the Ouachita Orogeny and the opening of the Gulf of Mexico are shown for reference. The shaded area corresponds to the temperature range for the partial annealing zone of apatite. The time-temperature estimation for box 1 is based on the assumption that rocks in the Llano and Arbuckle regions were at the surface during the early Permian. Box 2 is based on AFT data from the Llano and Arbuckle regions. Boxes 3, 4 and 5 are based on AFT data from the Wichita Mountians, Marathon Mountians and Benton uplift areas of the Ouachitas. The solid line represents the thermal history model that best fits the fission-track age and track length data (Winkler et al., 1999). Dashed lines a and b represent modeled AFT data from two samples located in the central Appalachians (Pennsylvania) for comparison to the Ouachitas (Blackmer et al., 1994).

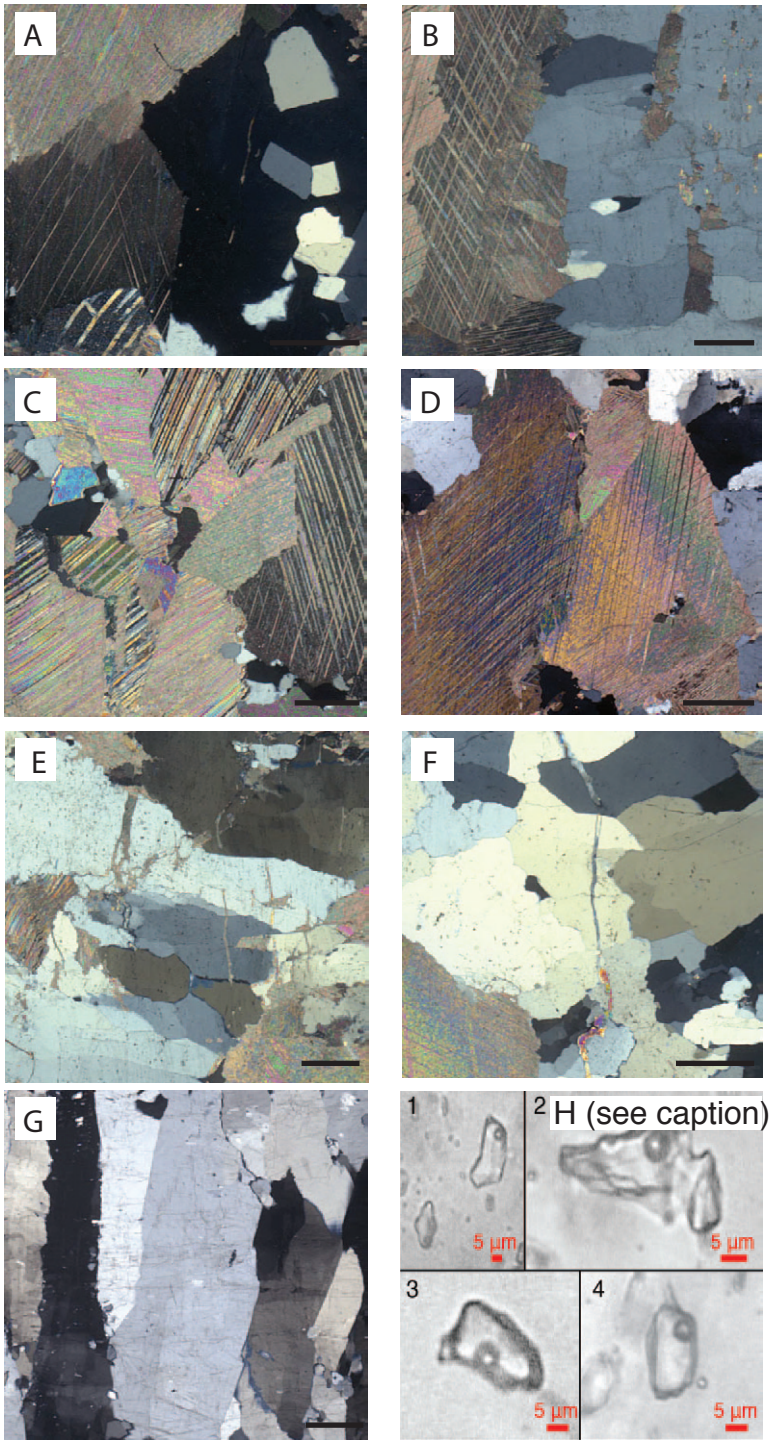

Fig. 7: Thin section photomicrographs of veins from the Ouachita Orogen. A) Sharp grain boundary, AR132. B) Feathered grain boundary, AR76. C) Twinned calcite, AR132. D) Twinned calcite, AR96. E) Healed fractures in quartz, AR76. F) Healed fractures in quartz, AR132. G) Fluid inclusion bands in fibrous quartz, AR119. H) Fluid inclusions from AR115 (1), AR128 (2), AR136 (3) and AR115 (4). Bar is 2mm unless otherwise noted.

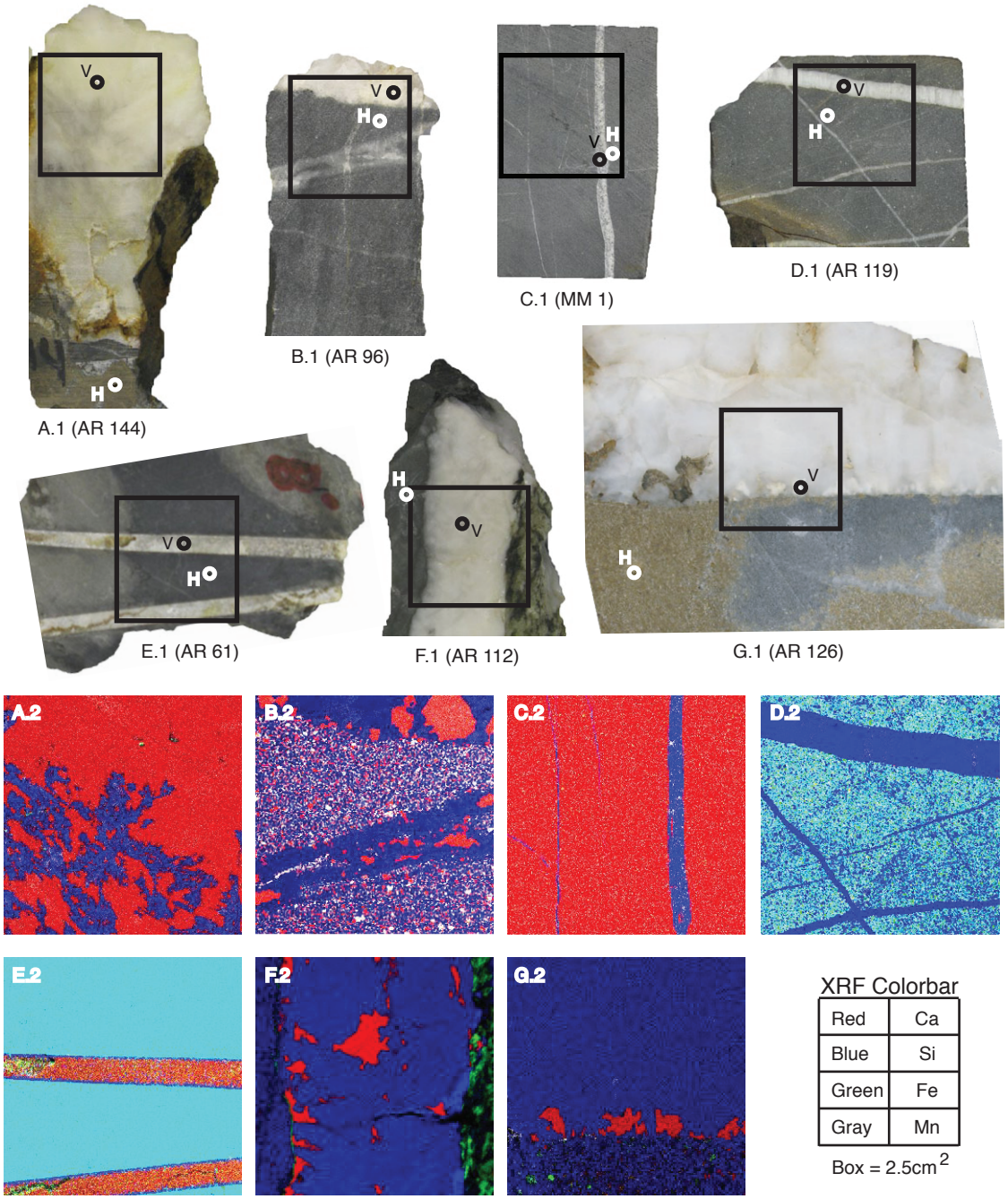

Fig. 8: XRF element maps and isotope sample locations. XRF maps are 2.5 cm2. Isotope samples are labeled as H (host) and V (vein) for each specimen.

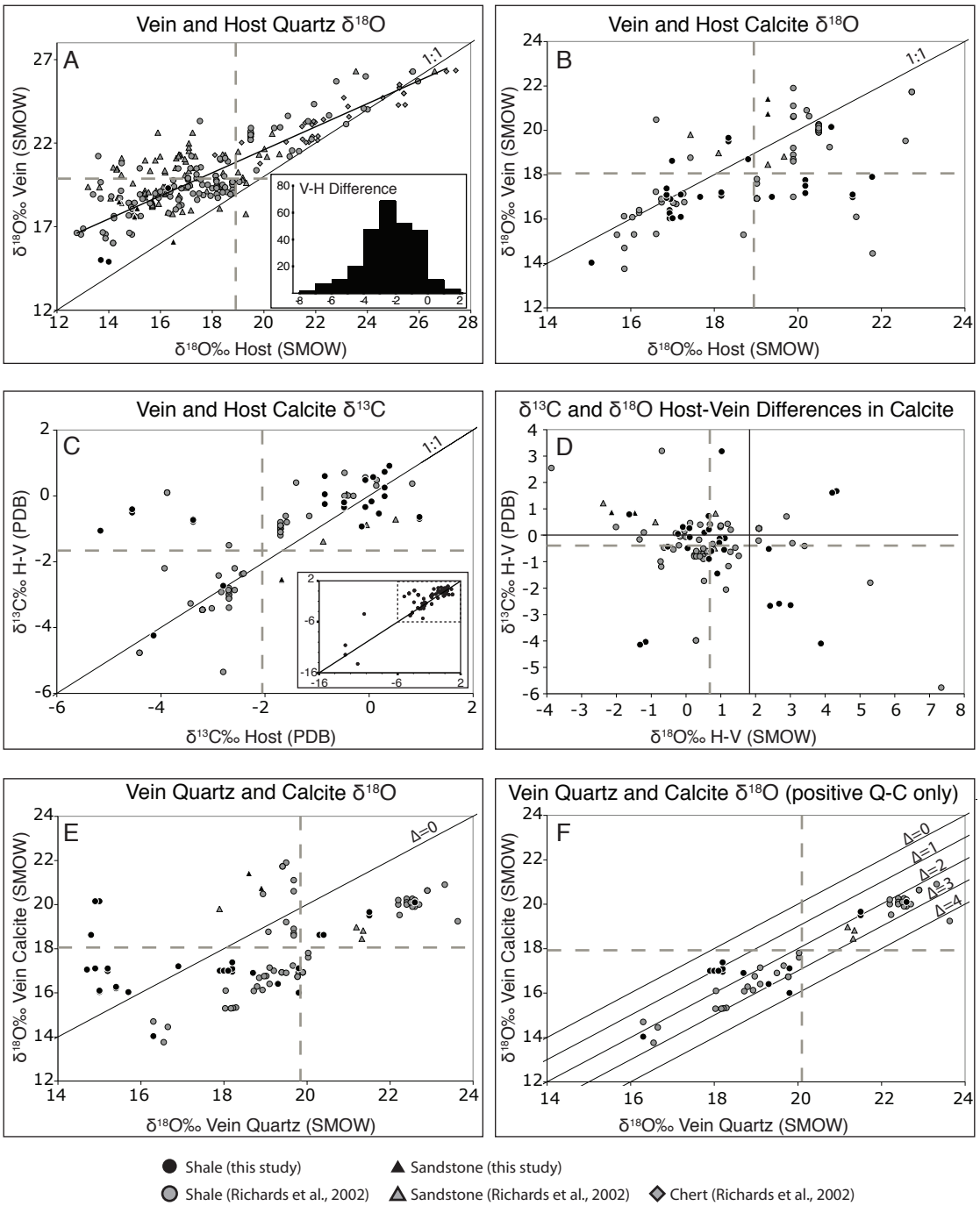

Fig. 9: Stable isotopic data from veins and adjacent host. Black-filled symbols, this study; gray-filled symbols, Richards et al. (2002). See text for discussion.

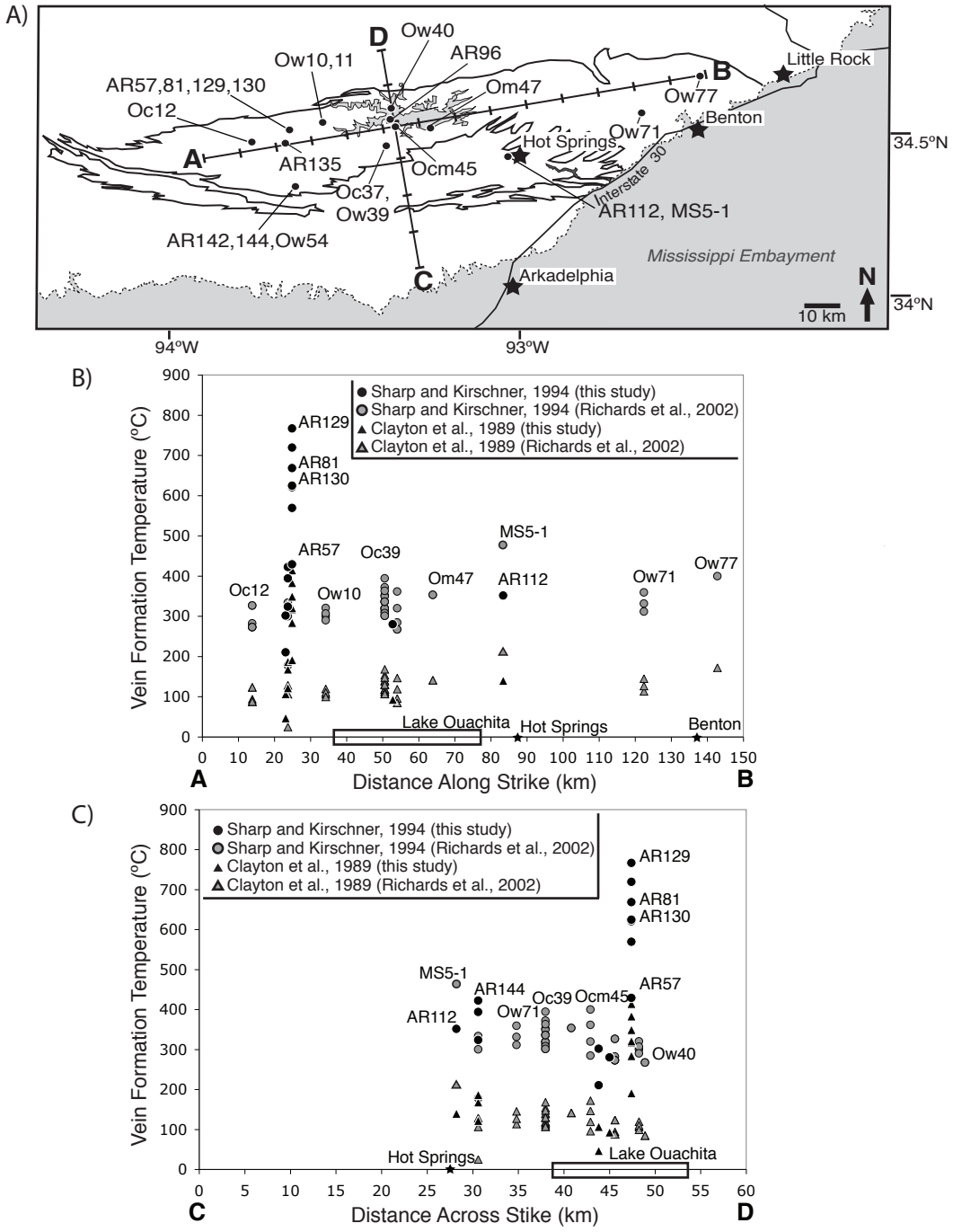

Fig. 10: Temperatures measured in veins plotted along strike (A-B) and across strike (C-D) of the Ouachita core. A) Generalized map of the Ouachita core with sample locations used for quartz-calcite isotope thermometry plotted. Samples labeled with AR are samples collected in Arkansas in this study. Samples labeled Oc (Collier shale), Om (Mazarn shale) and Ow (Womble shale) are samples collected by Richards et al. (2002). B) Vein precipitation temperatures along strike and C) Vein precipitation temperatures across strike.

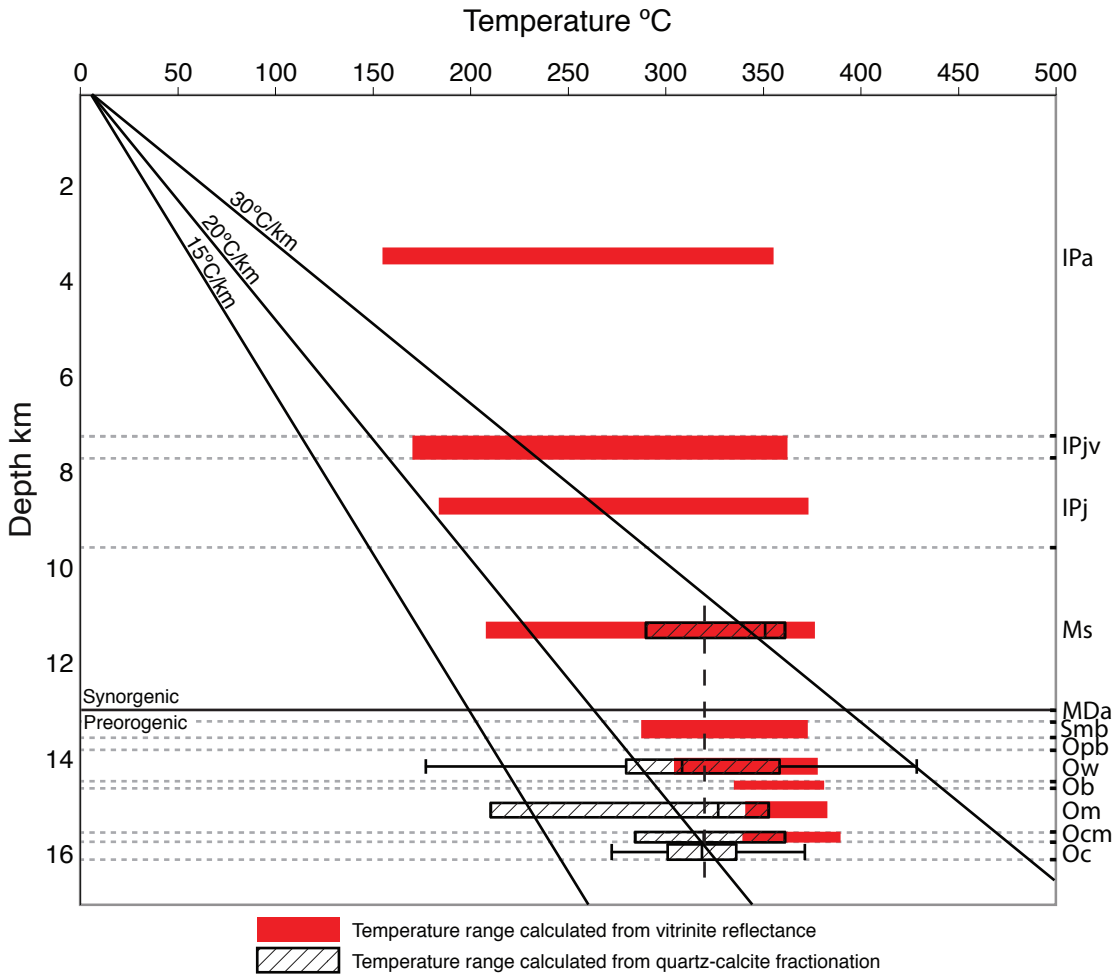

Fig. 11: Vitrinite reflectance and vein formation temperatures in each formation with depth. Dased line is average vein formation temperature. Geothermal gradients shown for reference. Formation names are abbreviated, see Figure 4.

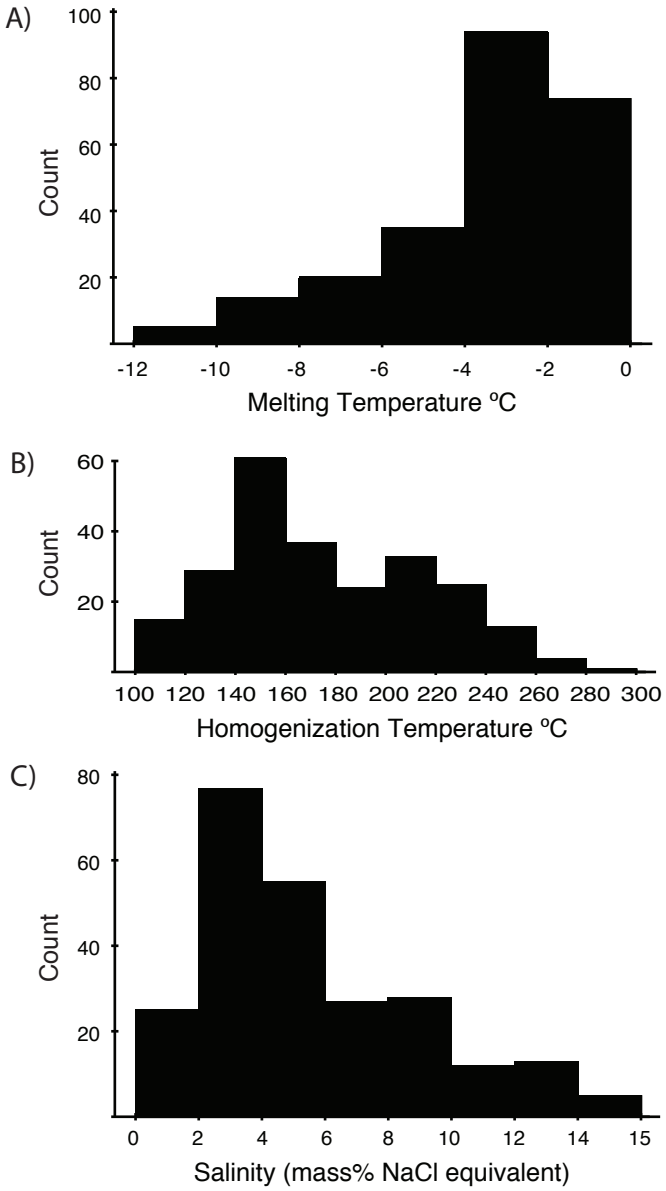

Fig. 12: Histograms for the melting temperatures (A), homogenization temperatures (B) and salinities (C) of all of the fluid inclusions.

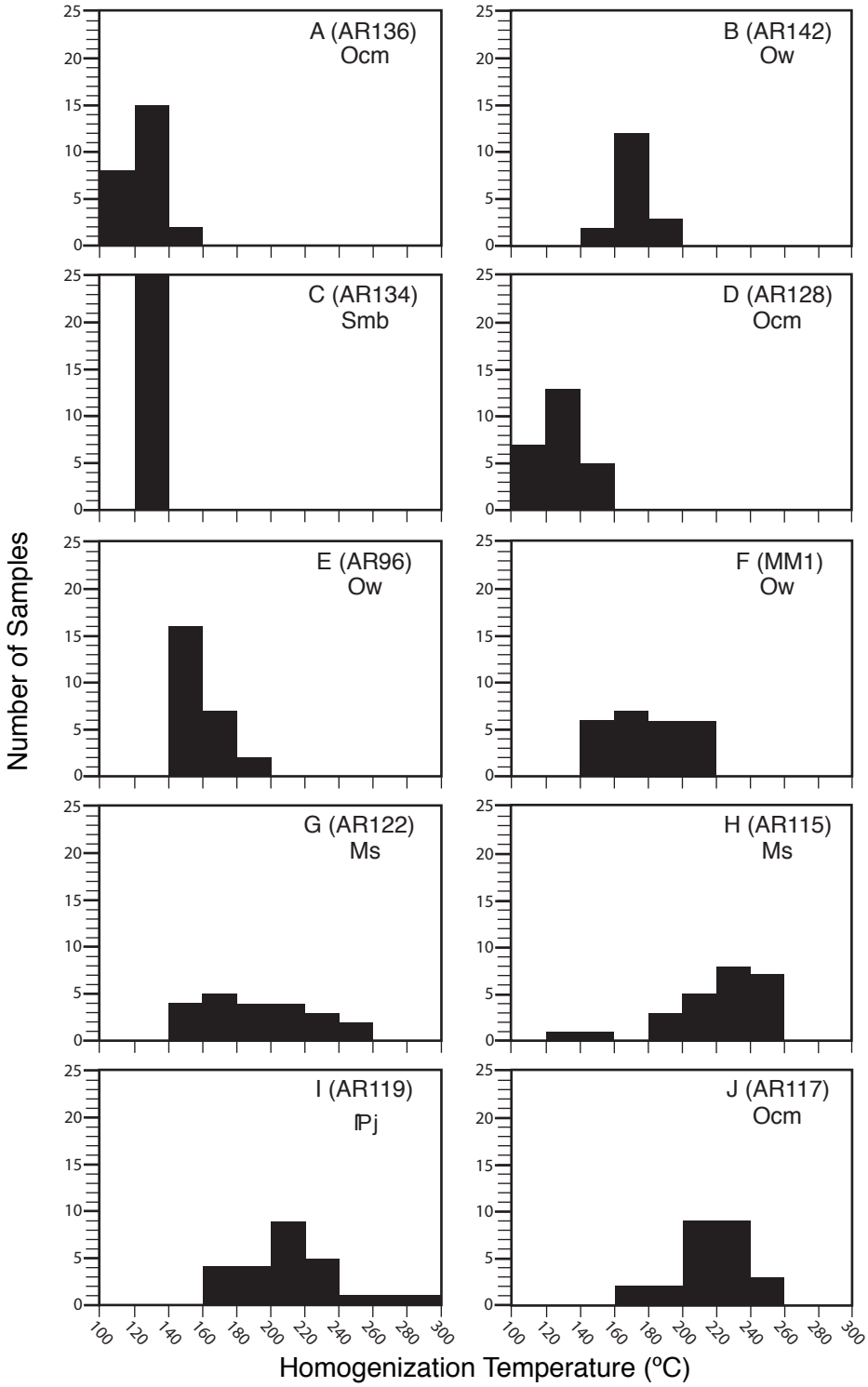

Fig. 13: Histograms of the homogenization temperatures for each fluid inclusion sample in west (AR136) to east (AR117) order. Key: Ocm (Crystal Mountain sandstone), Ow (Womble shale), Smb (Missouri Mtn. shale), Ms (Stanley shale) and Pj (Jackfork sandstone).

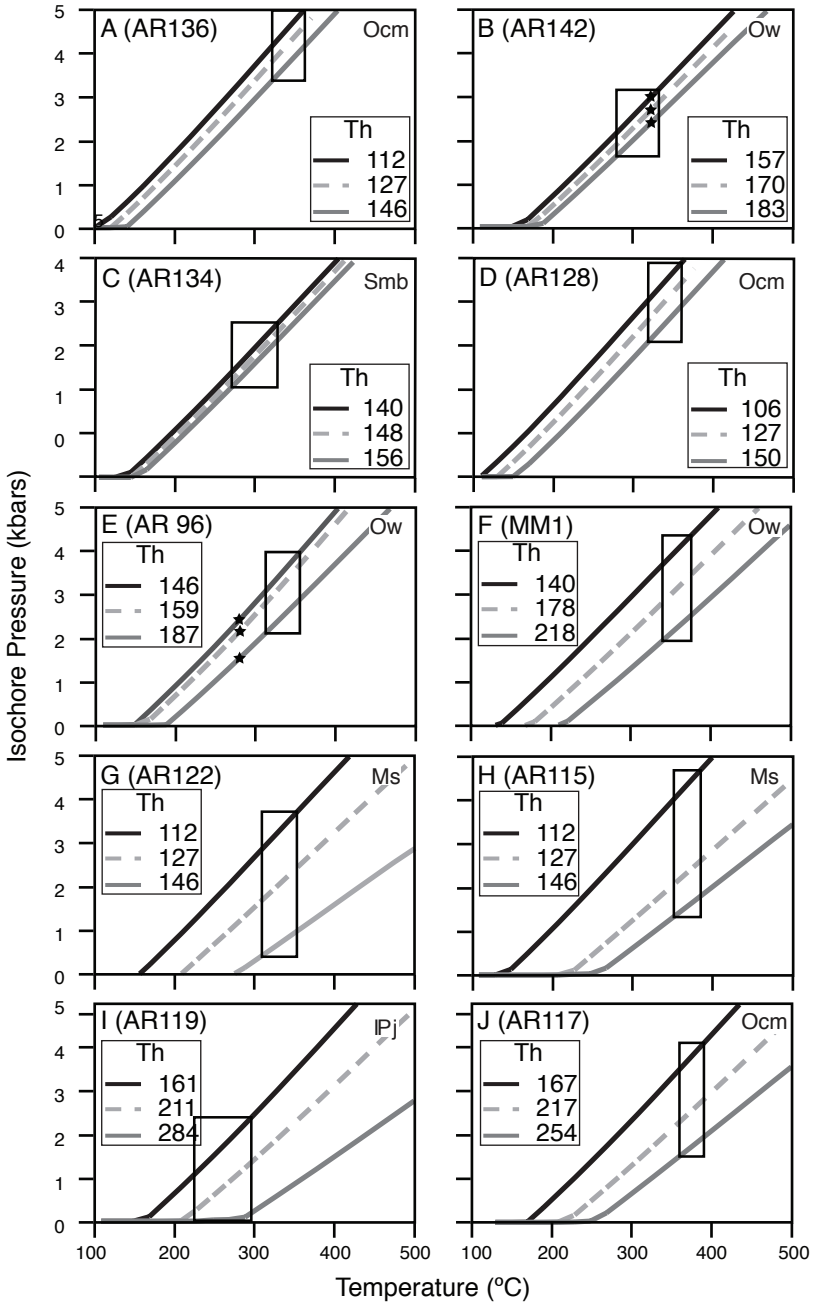

Fig. 14: Fluid inclusion isochores computed for each sample using the minimum, maximum and average homogenization temperatures. The homogenization temperatures used for each sample are listed in the box on each graph. The thick-lined boxes on each graph represent the pressure and temperature range of fluid inclusion formation based on vitrinite reflectance values for each sample. That is, the pressure limits are defined by the minimum and maximum isochore and the temperature limits are defined by the temperature calculated from vitrinite reflectance values using the calibration of Price (1983). The stars are temperature constraints using quartz-calcite fractionation and the equation of Sharp and Kirschner (1994) for AR96 and AR142. These are the only two fluid inclusion samples with isotopic temperature constraints. Key: Ocm (Crystal Mountain sandstone), Ow (Womble shale), Smb (Missouri Mtn. shale), Ms (Stanley shale) and Pj (Jackfork sandstone).

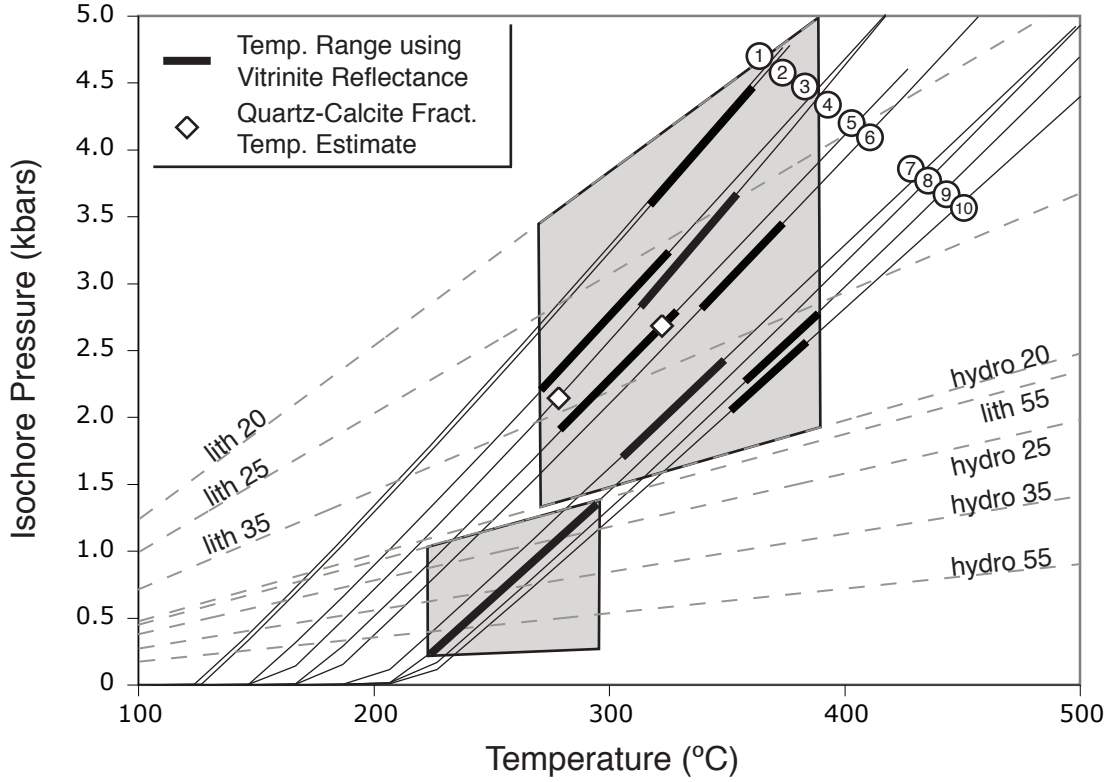

Fig. 15: Average isochores for each fluid inclusion sample versus multiple lithostatic and hydrostatic geothermal gradients. Isochores are labeled 1-10, where 1-AR128, 2-AR136, 3-134, 4-AR96, 5-AR142, 6-MM1, 7-AR122, 8-AR119, 9-AR117 and 10-AR115. Vein formation conditions correspond to lithostatic geothermal gradients of ~20º-55ºC/km using the temperatures calculated from Sharp and Kirschner, (1993). The exception to this trend is AR119, which corresponds to a hydrostatic geothermal gradient of ~25º-55ºC/km.

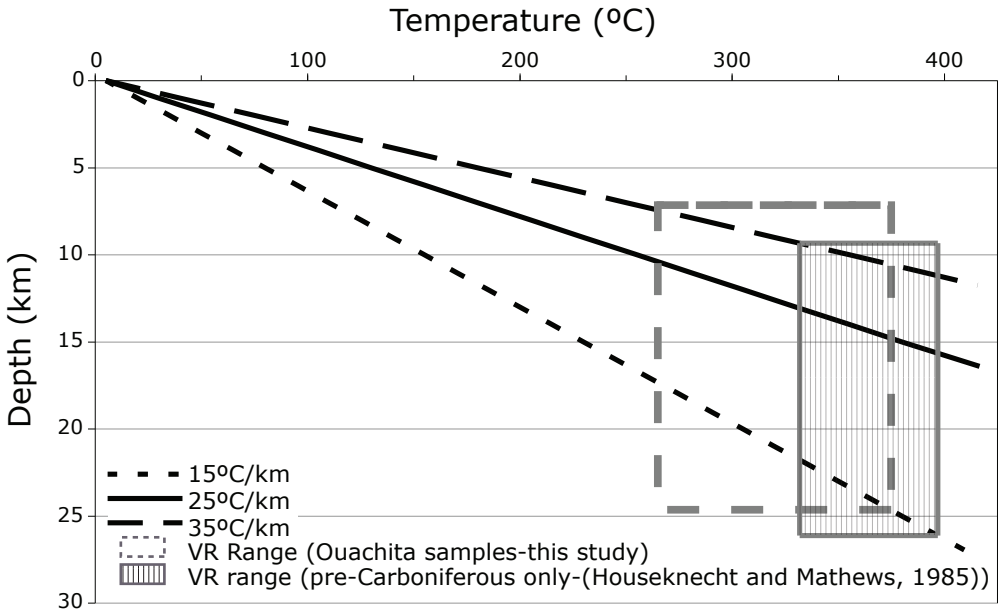

Fig. 16: Maximum depth constraints for vein formation using temperatures calculated from vitrinite reflectance, assuming geothermal gradients of 15º, 25º and 35ºC/km. The dashed box represents the maximum depths using the VR for all the samples in the study. The solid, filled box is the depth constraints calculated when using the VR of pre-Carboniferous strata only (from Houseknectht and Mathews, 1985).

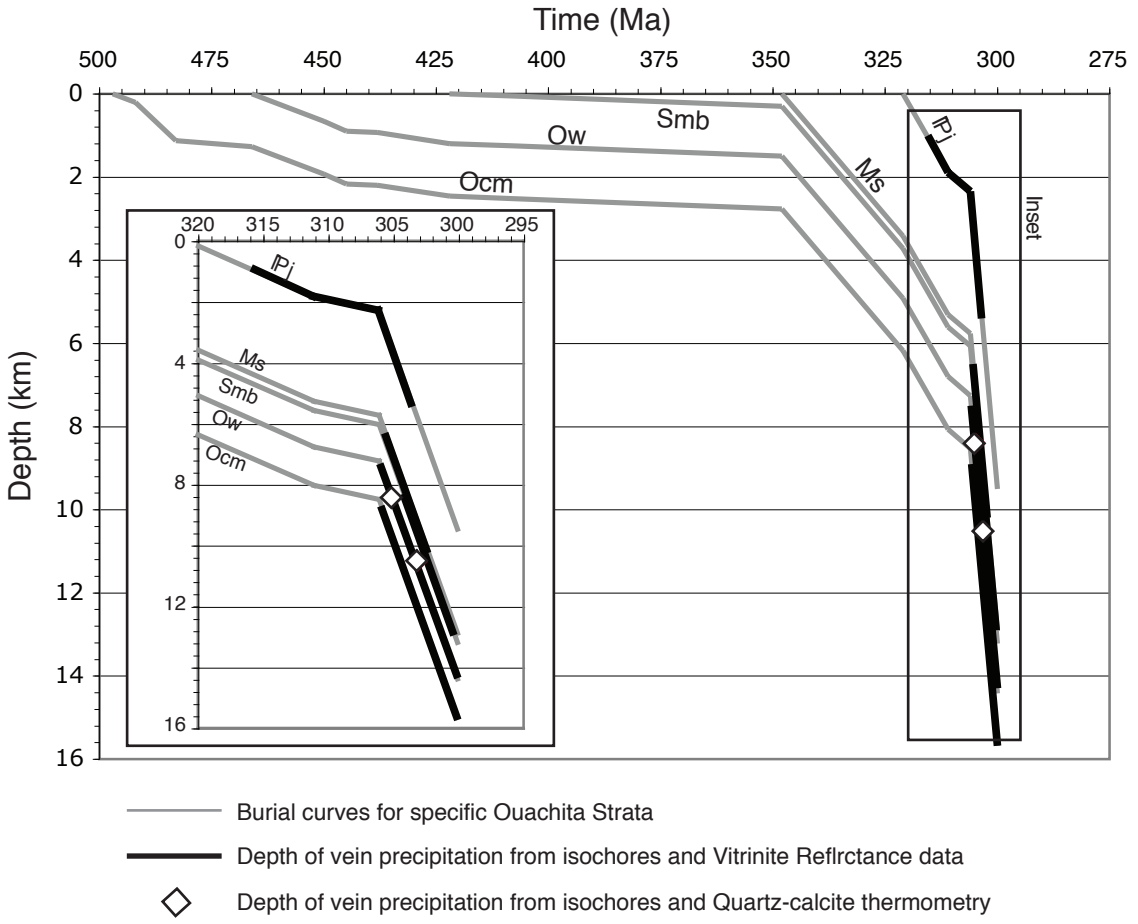

Fig. 17: Burial curves for selected formations in the Ouachitas, using core thickness values reported by Thomas (1977), Viele and Thomas (1989), and Arbenz (2009). Thick lines represent the depth of vein formation calculated from VR temperature constraints on the average isochore of each sample. The depths correspond to an age of vein emplacement of early to middle Pennsylvanian. Key: Ocm (Crystal Mountain sandstone), Ow (Womble shale), Smb (Missouri Mtn. shale), Ms (Stanley shale) and Pj (Jackfork sandstone).

APPENDIX B

TABLES

Table 1
Stable isotope analyses.

				Calcite				Quartz	
				Host		Vein		Host	Vein
Sample Name	Latitude (1)	Longitude (1)	Fm. Name (2)	$\delta^{18}O$ (SMOW)	$\delta^{13}C$ (PDB)	$\delta^{18}O$ (SMOW)	$\delta^{13}C$ (PDB)	$\delta^{18}O$ (SMOW)	$\delta^{18}O$ (SMOW)
AR032 a	34.46916	-93.08944	Ms						14.0
AR032 b	34.46916	-93.08944	Ms						14.2
AR057	34.56364	-93.66843	Ow	16.95	0.08	16.90	0.57		18.7
AR061 a	34.56364	-93.66843	Ow	20.18	-3.38	17.76	-0.71		
AR061 b	34.56364	-93.66843	Ow	20.18	-3.38	17.50	-0.79		
AR061 c	34.56364	-93.66843	Ow	20.18	-3.38	17.17	-0.73		
AR076 a	34.56364	-93.66843	Ow	18.17	-0.48	17.05	-0.37		14.7
AR076 b	34.56364	-93.66843	Ow	18.17	-0.48	17.20	-0.35		16.9
AR081 a	34.56364	-93.66843	Ow	19.38	0.39	17.00	0.91		17.9
AR081 b	34.56364	-93.66843	Ow	19.38	0.39	17.00	0.91		18.0
AR089 a	34.56364	-93.66843	Ow	21.31	0.97	16.98	-0.70		15.2
AR089 b	34.56364	-93.66843	Ow	21.31	0.97	17.11	-0.64		15.2
AR096 a	34.59718	-93.39856	Ow	16.93	-4.14	16.40	-4.24	11.8	19.3
AR096 b	34.59718	-93.39856	Ow	16.93	-4.14	16.40	-4.24	16.5	19.3
AR098 a	34.59718	-93.39856	Ow	16.99	-0.14	18.62	-0.93		20.3
AR098 b	34.59718	-93.39856	Ow	16.99	-0.14	18.62	-0.93		20.4
AR098 c	34.59718	-93.39856	Ow	16.99	-0.14	18.62	-0.93		14.8
AR099	34.59718	-93.39856	Ow	18.81	-2.80	18.70	-2.73		
AR100	34.59718	-93.39856	Ow	21.78	-5.16	17.90	-1.06		
AR108	34.23083	-93.09750	Mda						17.4
AR112	34.48583	-93.08722	Ms	15.06	-11.08	14.03	-14.26		16.3
AR114 a	34.47861	-93.11611	Ms						18.7
AR114 b	34.47861	-93.11611	Ms						19.0
AR115	34.47861	-93.11611	Ms						17.6
AR116	34.63361	-93.05833	Ob						18.8
AR117	34.67806	-93.07250	Ocm					15.1	18.1
AR119	34.85000	-93.09667	Pj						20.2
AR120	34.51139	-93.20639	Ms						14.5
AR122	34.51139	-93.20639	Ms						16.7
AR123 a	34.51139	-93.20639	Ms						13.7
AR123 b	34.51139	-93.20639	Ms						13.8
AR124	34.50583	-93.19667	Ms						15.7
AR125 b	34.50583	-93.19667	Mda						17.0
AR126 a	34.51500	-93.38306	Ob	19.28	-1.68	21.42	-2.56		18.6
AR126 b	34.51500	-93.38306	Ob	19.28	-1.68	20.75	-2.53		18.9
AR127	34.52444	-93.40167	Ocm					14.5	18.4
AR128	34.52444	-93.40167	Ocm					14.4	18.5
AR129 a	34.56361	-93.66833	Ow	16.86	0.30	16.95	-0.01		18.2
AR129 b	34.56361	-93.66833	Ow	16.86	0.30	17.09	0.25		18.2
AR129 c	34.56361	-93.66833	Ow	16.86	0.30	17.38	0.73		18.2
AR130	34.56361	-93.66833	Ow	17.66	0.05	17.00	-0.17		18.1
AR131 a	34.56500	-93.63139	Ow	16.93	-0.85	16.20	-0.25		15.4
AR131 b	34.56500	-93.63139	Ow	16.93	-0.85	16.03	0.60		15.7
AR131 c	34.56500	-93.63139	Ow	16.93	-0.85	16.27	0.05		15.4
AR132 a	34.56500	-93.63139	Ow	17.00	-0.48	16.02	-0.19		15.0
AR132 b	34.56500	-93.63139	Ow	17.00	-0.48	16.04	-0.20		15.0
AR133 a	34.56500	-93.63139	Ow	17.20	-0.07	17.10	-0.34		14.9
AR133 b	34.56500	-93.63139	Ow	17.20	-0.07	16.10	0.48		15.0
AR134	34.65056	-93.53278	Smb						25.0
AR135 a	34.52472	-93.67861	Smb			16.00	-0.40		19.8
AR135 b	34.52472	-93.67861	Smb			17.11	-0.34		19.8
AR136	34.52472	93.67861	Ocm						19.9
AR137	34.49917	-93.68833	Ocm					15.0	17.6
AR138	34.49917	-93.68833	Ocm						17.1
AR139	34.49917	-93.68833	Ocm						18.1
AR142	34.40750	-93.64833	Ow			20.10	-0.29		22.6
AR143	34.40750	-93.64833	Ow						21.4
AR144 a	34.40750	-93.64833	Ow	18.34	-4.55	19.50	-0.51		21.5
AR144 b	34.40750	-93.64833	Ow	18.34	-4.55	19.66	-0.41		21.5
MM1 a	34.67011	-93.21505	Ow	20.80	0.19	20.15	-0.54	13.7	15.0
MM1 b	34.67011	-93.21505	Ow	20.80	0.19	20.15	-0.54	14.0	14.9

(1) WGS84 datum used to identify latitude and longitude
(2) Formation Names: MDa, Arkansas Novaculite; Ob, Blakely Ss; Ocm, Crystal Mountain Ss; Pj, Jackfork Ss; Smb, Missouri Mountain Sh; Ms, Stanley Sh; Ow, Womble Sh

Table 2
Statistical analysis of isotope data.

			This study		Richards et al. (2002)		Combined*	
			Mean	std. dev.	mean	std. dev.	mean	std. dev.
		$\delta^{18}O$ (SMOW)	18.28	1.69	19.26	2.22	18.94	2.10
		$\delta^{13}C$ (PDB)	-1.45	2.45	-1.92	1.56	-2.05	2.53
		$\delta^{18}O$ (SMOW)	17.58	1.57	18.34	2.04	18.05	1.91
		$\delta^{13}C$ (PDB)	-1.01	2.51	-2.04	2.29	-1.65	2.41
		$\delta^{18}O$ (SMOW)	0.72	1.67	0.70	1.61	0.71	1.62
		$\delta^{13}C$ (PDB)	-0.38	1.63	0.17	2.39	-0.38	1.40
		$\delta^{18}O$ (SMOW)	14.59	1.41	19.07	4.10	18.94	4.11
		$\delta^{18}O$ (SMOW)	17.31	3.01	20.35	2.19	19.85	2.59
		$\delta^{18}O$ (SMOW)	-2.88	2.27	-2.38	1.65	-2.40	1.67
		$\delta^{18}O$ (SMOW)	-0.01	2.34	1.92	1.48	1.26	2.02
		$\delta^{18}O$ (SMOW) with positive fractionation	1.93	0.90	2.38	0.67	2.37	0.63

*Combined data includes isotope data from this study and that of Richards et al. (2002)

Table 3
Fluid inclusion analyses.

Sample Name	Tm* °C	Th* °C	Salinity (mass%)	Molality (mole/kg)	Density (g/cc)	Weight % H_2O
AR096 a	-6.2	146.4	9.488	1.793	1.079	90.51
AR096 a	-9.6	146.7	13.560	2.683	1.112	86.44
AR096 a	-3.7	147.1	5.998	1.091	1.051	94.00
AR096 a	-5.6	147.8	8.690	1.628	1.072	91.31
AR096 a	-4.5	148.2	7.162	1.320	1.060	92.84
AR096 a	-9.6	148.8	13.560	2.683	1.112	86.44
AR096 a	-9.3	150.5	13.231	2.608	1.109	86.77
AR096 a	-10.1	151.8	14.097	2.807	1.117	85.90
AR096 a	-3.9	152.2	6.293	1.149	1.053	93.71
AR096 a	-6.4	154.2	9.749	1.848	1.081	90.25
AR096 a	-10.9	154.5	14.924	3.001	1.124	85.08
AR096 a	-6.7	157.6	10.135	1.929	1.084	89.87
AR096 a	-9.6	157.9	13.560	2.683	1.112	86.44
AR096 a	-4.7	158.6	7.446	1.376	1.062	92.55
AR096 a	-9.1	158.9	13.008	2.558	1.107	86.99
AR096 a	-9.8	159.4	13.776	2.733	1.114	86.22
AR096 a	-10.1	162.0	14.097	2.807	1.117	85.90
AR096 a	-5.3	163.7	8.281	1.544	1.069	91.72
AR096 a	-9.2	165.8	13.120	2.583	1.108	86.88
AR096 a	-8.5	166.3	12.325	2.404	1.102	87.68
AR096 a	-5.0	167.4	7.867	1.460	1.066	92.13
AR096 a	-10.7	169.1	14.721	2.953	1.122	85.28
AR096 a	-10.5	172.4	14.515	2.904	1.120	85.48
AR096 a	-9.9	182.7	13.884	2.758	1.115	86.12
AR096 a	-4.4	187.6	7.019	1.291	1.059	92.98
AR115	-1.9	139.2	3.210	0.567	1.029	96.79
AR115	-1.2	159.8	2.061	0.360	1.021	97.94
AR115	-2.3	184.6	3.850	0.685	1.034	96.15
AR115	-1.8	189.5	3.048	0.538	1.028	96.95
AR115	-2.5	198.1	4.166	0.744	1.037	95.83
AR115	-2.8	211.2	4.633	0.831	1.040	95.37
AR115	-2.4	211.3	4.008	0.714	1.036	95.99
AR115	-2.4	213.8	4.008	0.714	1.036	95.99
AR115	-2.2	217.8	3.691	0.656	1.033	96.31
AR115	-2.8	219.1	4.633	0.831	1.040	95.37
AR115	-1.8	221.5	3.048	0.538	1.028	96.95
AR115	-1.0	222.9	1.726	0.300	1.018	98.27
AR115	-1.3	224.3	2.228	0.390	1.022	97.77
AR115	-2.9	227.8	4.788	0.860	1.042	95.21
AR115	-3.1	228.9	5.095	0.918	1.044	94.91
AR115	-1.6	229.6	2.722	0.479	1.026	97.28
AR115	-1.2	230.7	2.061	0.360	1.021	97.94
AR115	-2.1	231.4	3.532	0.626	1.032	96.47
AR115	-1.7	245.2	2.886	0.508	1.027	97.11
AR115	-2.3	246.7	3.850	0.685	1.034	96.15
AR115	-2.4	247.1	4.008	0.714	1.036	95.99
AR115	-2.2	251.8	3.691	0.656	1.033	96.31
AR115	-1.9	253.8	3.210	0.567	1.029	96.79
AR115	-2.5	256.4	4.166	0.744	1.037	95.83
AR115	-2.6	258.2	4.322	0.773	1.038	95.68
AR117	-5.6	167.9	8.690	1.628	1.072	91.31
AR117	-5.4	168.3	8.418	1.572	1.070	91.58
AR117	-5.8	188.4	8.959	1.683	1.074	91.04
AR117	-6.6	190.3	10.007	1.902	1.083	89.99
AR117	-4.1	203.0	6.585	1.206	1.056	93.41
AR117	-7.0	205.6	10.515	2.010	1.087	89.49
AR117	-5.6	207.5	8.690	1.628	1.072	91.31
AR117	-4.2	210.0	6.730	1.234	1.057	93.27
AR117	-5.1	211.0	8.006	1.489	1.067	91.99
AR117	-3.9	212.4	6.293	1.149	1.053	93.71
AR117	-7.9	218.4	11.618	2.249	1.096	88.38
AR117	-3.9	219.0	6.293	1.149	1.053	93.71
AR117	-8.4	219.6	12.209	2.379	1.101	87.79
AR117	-6.8	221.1	10.262	1.956	1.085	89.74
AR117	-5.2	223.4	8.144	1.517	1.068	91.86
AR117	-5.6	224.8	8.690	1.628	1.072	91.31
AR117	-8.3	228.8	12.092	2.353	1.100	87.91
AR117	-6.2	233.4	9.488	1.793	1.079	90.51

Table 3 Cont.

Sample Name	Tm* °C	Th* °C	Salinity (mass%)	Molality (mole/kg)	Density (g/cc)	Weight % H_2O
AR117	-4.9	234.7	7.727	1.432	1.065	92.27
AR117	-6.3	234.8	9.619	1.820	1.080	90.38
AR117	-3.8	234.9	6.146	1.120	1.052	93.85
AR117	-4.7	237.8	7.446	1.376	1.062	92.55
AR117	-6.4	241.3	9.749	1.848	1.081	90.25
AR117	-4.2	247.2	6.730	1.234	1.057	93.27
AR117	-3.7	254.0	5.998	1.091	1.051	94.00
AR119	-5.6	161.2	8.690	1.628	1.072	91.31
AR119	-7.9	167.2	11.618	2.249	1.096	88.38
AR119	-6.4	168.6	9.749	1.848	1.081	90.25
AR119	-9.2	169.5	13.120	2.583	1.108	86.88
AR119	-6.1	197.5	9.357	1.766	1.078	90.64
AR119	-3.2	197.6	5.247	0.947	1.045	94.75
AR119	-5.2	198.3	8.144	1.517	1.068	91.86
AR119	-4.6	199.2	7.304	1.348	1.061	92.70
AR119	-3.7	201.6	5.998	1.091	1.051	94.00
AR119	-5.2	202.9	8.144	1.517	1.068	91.86
AR119	-3.4	203.0	5.549	1.005	1.047	94.45
AR119	-8.1	204.7	11.856	2.301	1.098	88.14
AR119	-3.9	207.9	6.293	1.149	1.053	93.71
AR119	-5.6	209.6	8.690	1.628	1.072	91.31
AR119	-8.4	211.9	12.209	2.379	1.101	87.79
AR119	-6.9	212.3	10.389	1.983	1.086	89.61
AR119	-3.9	215.4	6.293	1.149	1.053	93.71
AR119	-7.8	223.4	11.498	2.222	1.095	88.50
AR119	-6.8	224.2	10.262	1.956	1.085	89.74
AR119	-5.4	225.3	8.418	1.572	1.070	91.58
AR119	-7.1	227.4	10.640	2.037	1.088	89.36
AR119	-7.7	230.7	11.378	2.196	1.094	88.62
AR119	-6.1	253.1	9.357	1.766	1.078	90.64
AR119	-6.1	271.4	9.357	1.766	1.078	90.64
AR119	-4.3	284.5	6.875	1.263	1.058	93.13
AR122	-1.2	147.9	2.061	0.360	1.021	97.94
AR122	-3.1	153.2	5.095	0.918	1.044	94.91
AR122	-1.6	153.5	2.722	0.479	1.026	97.28
AR122	-4.1	156.2	6.585	1.206	1.056	93.41
AR122	-2.3	160.7	3.850	0.685	1.034	96.15
AR122	-2.9	167.1	4.788	0.860	1.042	95.21
AR122	-2.2	169.3	3.691	0.656	1.033	96.31
AR122	-0.8	175.1	1.387	0.241	1.016	98.61
AR122	-0.9	177.1	1.557	0.271	1.017	98.44
AR122	-0.6	182.9	1.046	0.181	1.013	98.95
AR122	-1.4	188.7	2.393	0.419	1.023	97.61
AR122	-1.8	188.8	3.048	0.538	1.028	96.95
AR122	-1.2	189.3	2.061	0.360	1.021	97.94
AR122	-1.4	201.2	2.393	0.419	1.023	97.61
AR122	-0.3	202.7	0.527	0.091	1.009	99.47
AR122	-0.7	203.1	1.217	0.211	1.014	98.78
AR122	-0.4	217.6	0.701	0.121	1.011	99.30
AR122	-1.2	225.6	2.061	0.360	1.021	97.94
AR122	-1.0	234.9	1.726	0.300	1.018	98.27
AR122	-1.8	235.7	3.048	0.538	1.028	96.95
AR122	-2.4	240.2	4.008	0.714	1.036	95.99
AR122	-1.7	243.1	2.886	0.508	1.027	97.11
AR122	-0.9	263.6	1.557	0.271	1.017	98.44
AR122	-0.6	267.4	1.046	0.181	1.013	98.95
AR122	-0.3	271.5	0.527	0.091	1.009	99.47
AR128	-0.2	105.6	0.352	0.061	1.008	99.65
AR128	-0.7	106.7	1.217	0.211	1.014	98.78
AR128	-0.2	108.4	0.352	0.061	1.008	99.65
AR128	-0.1	109.3	0.177	0.030	1.007	99.82
AR128	-0.7	109.4	1.217	0.211	1.014	98.78
AR128	-0.9	115.3	1.557	0.271	1.017	98.44
AR128	-2.6	118.9	4.322	0.773	1.038	95.68
AR128	-1.9	120.7	3.210	0.567	1.029	96.79
AR128	-2.0	121.9	3.371	0.597	1.031	96.63
AR128	-2.7	122.1	4.478	0.802	1.039	95.52
AR128	-2.2	124.2	3.691	0.656	1.033	96.31
AR128	-1.2	124.6	2.061	0.360	1.021	97.94

Table 3 Cont.

Sample Name	Tm* °C	Th* °C	Salinity (mass%)	Molality (mole/kg)	Density (g/cc)	Weight % H_2O
AR128	-2.4	125.9	4.008	0.714	1.036	95.99
AR128	-2.5	127.6	4.166	0.744	1.037	95.83
AR128	-2.9	128.7	4.788	0.860	1.042	95.21
AR128	-2.6	130.5	4.322	0.773	1.038	95.68
AR128	-2.2	134.3	3.691	0.656	1.033	96.31
AR128	-2.3	134.5	3.850	0.685	1.034	96.15
AR128	-3.0	138.6	4.942	0.889	1.043	95.06
AR128	-1.2	139.6	2.061	0.360	1.021	97.94
AR128	-2.7	142.7	4.478	0.802	1.039	95.52
AR128	-2.3	144.3	3.850	0.685	1.034	96.15
AR128	-3.2	144.8	5.247	0.947	1.045	94.75
AR128	-3.2	145.4	5.247	0.947	1.045	94.75
AR128	-3.3	149.5	5.398	0.976	1.046	94.60
AR134	-1.8	140.1	3.048	0.538	1.028	96.95
AR134	-2.0	141.2	3.371	0.597	1.031	96.63
AR134	-1.0	141.2	1.726	0.300	1.018	98.27
AR134	-2.9	141.4	4.788	0.860	1.042	95.21
AR134	-1.5	141.7	2.558	0.449	1.024	97.44
AR134	-2.2	141.9	3.691	0.656	1.033	96.31
AR134	-2.7	142.4	4.478	0.802	1.039	95.52
AR134	-1.9	143.9	3.210	0.567	1.029	96.79
AR134	-1.1	144.5	1.894	0.330	1.019	98.11
AR134	-2.1	145.5	3.532	0.626	1.032	96.47
AR134	-3.2	146.2	5.247	0.947	1.045	94.75
AR134	-1.6	146.7	2.722	0.479	1.026	97.28
AR134	-2.7	148.2	4.478	0.802	1.039	95.52
AR134	-2.0	149.3	3.371	0.597	1.031	96.63
AR134	-1.9	151.7	3.210	0.567	1.029	96.79
AR134	-1.9	151.7	3.210	0.567	1.029	96.79
AR134	-1.8	152.6	3.048	0.538	1.028	96.95
AR134	-1.6	153.8	2.722	0.479	1.026	97.28
AR134	-1.7	154.1	2.886	0.508	1.027	97.11
AR134	-3.6	154.7	5.849	1.063	1.050	94.15
AR134	-2.0	154.7	3.371	0.597	1.031	96.63
AR134	-1.7	155.2	2.886	0.508	1.027	97.11
AR134	-2.5	155.4	4.166	0.744	1.037	95.83
AR134	-2.1	155.6	3.532	0.626	1.032	96.47
AR134	-2.0	156.3	3.371	0.597	1.031	96.63
AR136	-1.6	111.6	2.722	0.479	1.026	97.28
AR136	-0.2	114.7	0.352	0.061	1.008	99.65
AR136	-1.9	114.8	3.210	0.567	1.029	96.79
AR136	-2.1	117.2	3.532	0.626	1.032	96.47
AR136	-2.9	118.1	4.788	0.860	1.042	95.21
AR136	-2.1	118.4	3.532	0.626	1.032	96.47
AR136	-0.4	119.1	0.701	0.121	1.011	99.30
AR136	-2.2	119.4	3.691	0.656	1.033	96.31
AR136	-0.9	124.3	1.557	0.271	1.017	98.44
AR136	-1.9	124.9	3.210	0.567	1.029	96.79
AR136	-2.2	127.2	3.691	0.656	1.033	96.31
AR136	-2.6	127.6	4.322	0.773	1.038	95.68
AR136	-2.4	128.4	4.008	0.714	1.036	95.99
AR136	-1.2	129.1	2.061	0.360	1.021	97.94
AR136	-2.2	131.5	3.691	0.656	1.033	96.31
AR136	-2.4	131.9	4.008	0.714	1.036	95.99
AR136	-2.2	132.6	3.691	0.656	1.033	96.31
AR136	-2.3	133.4	3.850	0.685	1.034	96.15
AR136	-1.8	133.8	3.048	0.538	1.028	96.95
AR136	-1.1	134.1	1.894	0.330	1.019	98.11
AR136	-1.8	134.7	3.048	0.538	1.028	96.95
AR136	-2.8	135.2	4.633	0.831	1.040	95.37
AR136	-2.8	139.3	4.633	0.831	1.040	95.37
AR136	-2.0	140.2	3.371	0.597	1.031	96.63
AR136	-2.2	145.8	3.691	0.656	1.033	96.31
AR142	-2.4	157.4	4.008	0.714	1.036	95.99
AR142	-2.8	159.2	4.633	0.831	1.040	95.37
AR142	-3.2	161.9	5.247	0.947	1.045	94.75
AR142	-2.3	163.7	3.850	0.685	1.034	96.15
AR142	-2.2	165.6	3.691	0.656	1.033	96.31
AR142	-2.3	166.4	3.850	0.685	1.034	96.15

Table 3 Cont.

Sample Name	Tm* °C	Th* °C	Salinity (mass%)	Molality (mole/kg)	Density (g/cc)	Weight % H_2O
AR142	-1.9	166.8	3.210	0.567	1.029	96.79
AR142	-2.1	167.4	3.532	0.626	1.032	96.47
AR142	-1.9	168.3	3.210	0.567	1.029	96.79
AR142	-2.2	171.4	3.691	0.656	1.033	96.31
AR142	-3.1	172.9	5.095	0.918	1.044	94.91
AR142	-2.9	173.4	4.788	0.860	1.042	95.21
AR142	-1.8	176.5	3.048	0.538	1.028	96.95
AR142	-2.0	176.9	3.371	0.597	1.031	96.63
AR142	-2.4	180.1	4.008	0.714	1.036	95.99
AR142	-2.4	180.5	4.008	0.714	1.036	95.99
AR142	-2.1	182.8	3.532	0.626	1.032	96.47
MM1 a	-0.9	140.1	1.557	0.271	1.017	98.44
MM1 a	-2.7	148.0	4.478	0.802	1.039	95.52
MM1 a	-0.4	154.1	0.701	0.121	1.011	99.30
MM1 a	-2.6	154.4	4.322	0.773	1.038	95.68
MM1 a	-2.0	158.9	3.371	0.597	1.031	96.63
MM1 a	-2.4	159.7	4.008	0.714	1.036	95.99
MM1 a	-4.1	165.8	6.585	1.206	1.056	93.41
MM1 a	-5.0	167.3	7.867	1.460	1.066	92.13
MM1 a	-2.6	167.9	4.322	0.773	1.038	95.68
MM1 a	-3.8	168.4	6.146	1.120	1.052	93.85
MM1 a	-3.8	171.2	6.146	1.120	1.052	93.85
MM1 a	-3.6	171.3	5.849	1.063	1.050	94.15
MM1 a	-3.7	174.2	5.998	1.091	1.051	94.00
MM1 a	-5.3	184.1	8.281	1.544	1.069	91.72
MM1 a	-5.1	185.5	8.006	1.489	1.067	91.99
MM1 a	-3.9	187.6	6.293	1.149	1.053	93.71
MM1 a	-5.7	189.2	8.825	1.656	1.073	91.18
MM1 a	-4.4	189.4	7.019	1.291	1.059	92.98
MM1 a	-3.9	191.1	6.293	1.149	1.053	93.71
MM1 a	-5.5	200.9	8.554	1.600	1.071	91.45
MM1 a	-3.1	201.1	5.095	0.918	1.044	94.91
MM1 a	-4.7	201.9	7.446	1.376	1.062	92.55
MM1 a	-3.4	202.5	5.549	1.005	1.047	94.45
MM1 a	-1.4	203.4	2.393	0.419	1.023	97.61
MM1 a	-5.8	217.8	8.959	1.683	1.074	91.04

*Tm - Melting temperature; Th - Homogenization temperature

Table 4
Vein emplacement conditions.

Sample	Fm.*	Ro min. ºC	Ro max. ºC	P min. (kbar)	P max. (kbar)	Depth min. (km)	Depth max. (km)
AR136	Ocm	322	363	3.85	4.67	14.82	17.98
AR142	Ow	278	332	1.94	2.95	7.47	11.36
AR134	Smb	272	327	2.22	3.34	8.55	12.86
AR128	Ocm	318	359	3.61	4.49	13.90	17.29
AR96	Ow	313	356	2.85	3.72	10.97	14.32
MM1	Ow	340	376	2.84	3.48	10.94	13.40
AR122	Ms	308	352	1.69	2.46	6.51	9.47
AR115	Ms	352	385	2.08	2.65	8.01	10.20
AR119	Pj	222	297	0.27	1.40	1.04	5.39
AR117	Ocm	359	391	2.30	2.83	8.86	10.90

*Formation Names: Ocm, Crystal Mountain Ss; Pj, Jackfork Ss; Smb, Missouri Mountain Sh; Ms, Stanley Sh; Ow, Womble Sh

VITA

Name: Jennifer Ann Piper

Address: Exxonmobil Exploration Company
233 Benmar Drive
Houston, TX 77060

Email Address: jennifer.a.piper@exxonmobil.com

Education: B.S., Geology, San Diego State University, 2008
M.S., Geology, Texas A&M University, 2011